AIAA SciTech Forum
4-8 January 2016, San Diego, California, USA
54th AIAA Aerospace Sciences Meeting

Trade Study of 3D Co-Flow Jet Wing for Cruise and Takeoff/Landing Performance

Alexis Lefebvre *, G.-C. Zha †
Dept. of Mechanical and Aerospace Engineering
University of Miami
Coral Gables, Florida 33124
E-mail: gzha@miami.edu

Abstract

This paper presents a trade study of co-flow jet (CFJ) flow control wings. Several geometry parameters are studied, including injection and suction locations, cavity configurations, airfoil thickness and wing aspect ratio. The simulations are performed at Mach number 0.10 and 0.15 to simulate the takeoff/landing, and cruise condition of a general aviation aircraft. Unlike the conventional flaps and slats systems or other active flow control techniques, CFJ wings contains no moving part and can be used for both cruise and takeoff/landing. A low C_μ with low energy expenditure can be used at cruise and high C_μ with very high lift can be used for takeoff/landing. At cruise, the CFJ wing with a 21% thickness achieves a maximum aerodynamic L/D of 38.8 at a remarkably high C_L of 1.22. When the CFJ pumping power P is taken into account, the corrected aerodynamic efficiency defined as $L/(D + P/V_\infty)$ is 25.2 at $AoA = 5^\circ$ and C_μ of 0.04. The takeoff/landing performance is also excellent with a maximum C_L of 4.7 achieved at C_μ of 0.28 and AoA of 40.0°. For both cruise and takeoff/landing, the CFJ wing moment is low and hence small tail force is needed for trimming purpose. CFJ is particularly advantageous to be used with thick airfoil such as 21% to achieve high cruise lift coefficient and high aerodynamic efficiency. For the 21% thickness airfoil, the CFJ wing has a drop of peak aerodynamic efficiency of 5.5%, but has the lift coefficient increase by 110%. A thick airfoil also provides higher structure strength, lighter weight, and more inner volume. This study demonstrates that the CFJ airfoil is not only very effective to drastically increase the maximum lift, but also able to achieve high aerodynamic efficiency with very high lift at cruise condition at a small angle of attack due to its low energy expenditure.

Overall the CFJ wing is particularly suitable for a light and compact wing with ultra-high wing loading and high efficiency. The extraordinary CFJ wing performance may bring a radically different design philosophy to revolutionize the future aircraft design. The CFJ wing will open a door to a new class of aircraft design.

Nomenclature

CFJ	Co-flow jet
AoA	Angle of attack
LE	Leading Edge
TE	Trailing Edge
S	Planform area
c	Profile chord
U	Flow velocity
q	Dynamic pressure $0.5\,\rho\,U^2$

* Graduate Student
† Professor, AIAA Associate Fellow

p	Static pressure
ρ	Air density
$\dot{m}$	Mass flow
M	Mach number
ω	Pitching Moment
P	Pumping power
∞	Free stream conditions
$_j$	Jet conditions
C_L	Lift coefficient $L/(q_\infty S)$
C_D	Drag coefficient $D/(q_\infty S)$
C_M	Moment coefficient $\omega/(q_\infty S\, c)$
C_p	Pressure coefficient $(p - p_\infty)/q_\infty$
C_μ	Jet momentum coef. $\dot{m}_j U_j/(q_\infty S)$
$(L/D)_c$	CFJ airfoil corrected efficiency $L/(D + P/V_\infty)$
Pc	Power coefficient $L/(q_\infty S V_\infty)$

1 Introduction

Active flow control (AFC) has attracted a lot of interest in the past three decades as a means to enhance the performance of airfoil, which otherwise has appeared to be saturated based on conventional configuration optimization. The AFC airfoil techniques that have been actively studied include circulation control (CC) airfoil[1, 2, 3], synthetic jet[4], plasma actuator jet, and the recently developed co-flow jet(CFJ) airfoil[5, 6, 7, 8, 9, 10, 11, 12, 13, 14, 15]. Most of the AFC airfoil techniques are aimed at improving the performance near stall or beyond stall to expand the operating range of the airfoil and augment the maximum lift. Few active flow controls are able to achieve airfoil performance improvement for cruise at low angle of attack (AoA). For example, the CC airfoil will have high cruise drag due to the blunt trailing edge or flap to have the Coanda effect. In addition, the blowing only on the CC airfoil has high energy expenditure that results extra drag due to withdrawing the mass flow from freestream[6]. The synthetic jet and plasma jet methodology are not clear if their perturbations are effective when the flow is well attached at a small AoA. The only AFC airfoil technique that is demonstrated to have excellent cruise performance is the CFJ airfoil due to its low energy expenditure [6, 11, 12, 16].

The CFJ airfoil is a zero-net mass-flux(ZNMF)flow control method recently developed by Zha et al. [5, 6, 7, 8, 9, 10, 11, 12, 13, 14, 15]. It is demonstrated to achieve radical lift augmentation, stall margin increase, drag reduction and moderate nose-down moment for stationary and pitching airfoils. In the CFJ airfoil concept, an injection slot near the leading edge (LE) and a suction slot near the trailing edge (TE) on the airfoil suction surface are created as sketched in Fig. 1. A small amount of mass flow is withdrawn into the airfoil near the TE, pressurized and energized by a pumping system inside the airfoil, and then injected near the LE tangentially to the main flow. The whole process does not add any mass flow to the system and hence is a ZNMF flow control.

Recently, two parametric studies were conducted by Lefebvre and Zha[14, 15] on several geometric parameters to better understand the performance potential of 2D CFJ airfoils. This article expands the previous investigations to 3D CFJ wings focusing on cruise performance. First, a CFJ wing equipped with the NACA 6415 CFJ airfoil is simulated. This case is of particular importance due to the availability of 2D experimental and computational results that can be used for reference and comparison [9, 12, 17, 18]. Then the CFJ location, injection and suction cavities geometry, airfoil thickness and wing aspect ratio are studied.

The ultimate goal of the trade study in this paper is to generate a CFJ wing with high cruise wing loading, high aerodynamic efficiency, high maximum lift coefficient, low moment, and low power consumption. This study lays the foundation to design a revolutionary general aviation electric aircraft, which has the potential

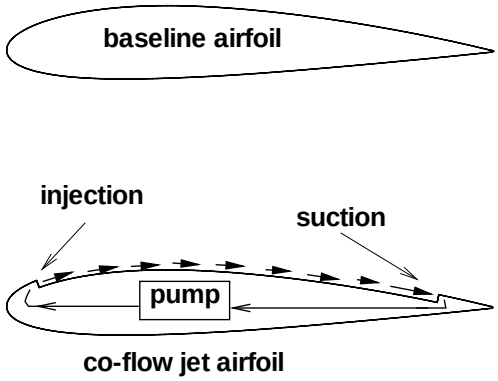

Figure 1: CFJ airfoil concept

to double the range of a same size electric aircraft using conventional design [16].

2 CFJ Parameters

This section introduces the definitions of several parameters that are used to describe CFJ wing performance.

2.1 Lift and Drag Calculation

The momentum and pressure at the injection and suction slots produce a reactionary force, which is automatically measured by the force balance in wind tunnel testing. However, for CFD simulation, the full reactionary force needs to be included. Using control volume analysis, the reactionary force can be calculated using the flow parameters at the injection and suction slot opening surfaces. Zha et al. [6] give the following formulations to calculate the lift and drag due to the jet reactionary force for a CFJ airfoil. By considering the effects of injection and suction jets on the CFJ airfoil, the expressions for these reactionary forces are given as :

$$F_{x_{cfj}} = (\dot{m}_j V_{j1} + p_{j1} A_{j1}) * cos(\theta_1 - \alpha) - (\dot{m}_j V_{j2} + p_{j2} A_{j2}) * cos(\theta_2 + \alpha) \tag{1}$$

$$F_{y_{cfj}} = (\dot{m}_{j1} V_{j1} + p_{j1} A_{j1}) * sin(\theta_1 - \alpha) + (\dot{m}_{j2} V_{j2} + p_{j2} A_{j2}) * sin(\theta_2 + \alpha) \tag{2}$$

where the subscripts 1 and 2 stand for the injection and suction respectively, and θ_1 and θ_2 are the angles between the injection and suction slot's surface and a line normal to the airfoil chord. α is the angle of attack.

The total lift and drag on the airfoil can then be expressed as:

$$D = R'_x - F_{x_{cfj}} \tag{3}$$

$$L = R'_y - F_{y_{cfj}} \tag{4}$$

where R'_x and R'_y are the surface integral of pressure and shear stress in x (drag) and y (lift) direction excluding the internal ducts of injection and suction. For CFJ wing simulations, the total lift and drag are calculated by integrating Eqs.(3) and (4) in the spanwise direction.

2.2 Jet Momentum Coefficient

The jet momentum coefficient C_μ is a parameter used to quantify the jet intensity. It is defined as:

$$C_\mu = \frac{\dot{m}V_j}{\frac{1}{2}\rho_\infty {V_\infty}^2 S} \tag{5}$$

where $\dot{m}$ is the injection mass flow, V_j is the mass-averaged injection velocity, ρ_∞ and V_∞ denote the free stream density and velocity, and S is the planform area.

2.3 Power Coefficient

CFJ is implemented by mounting a pumping system inside the wing that withdraws air from the suction slot and blows it into the injection slot. The power consumption is determined by the jet mass flow and total enthalpy change as the following:

$$P = \dot{m}(H_{t1} - H_{t2}) \tag{6}$$

where H_{t1} and H_{t2} are the mass-averaged total enthalpy in the injection cavity and suction cavity respectively, P is the Power required by the pump and $\dot{m}$ the jet mass flow rate. Introducing P_{t1} and P_{t2} the mass-averaged total pressure in the injection and suction cavity respectively, the pump efficiency η, and the total pressure ratio of the pump $\Gamma = \frac{P_{t1}}{P_{t2}}$, the power consumption is expressed as:

$$P = \frac{\dot{m}C_pT_{t2}}{\eta}(\Gamma^{\frac{\gamma-1}{\gamma}} - 1) \tag{7}$$

where γ is the specific heat ratio equal to 1.4 for air. The power coefficient is expressed as:

$$P_c = \frac{P}{\frac{1}{2}\rho_\infty V_\infty^3 S} \tag{8}$$

2.4 Corrected Aerodynamic Efficiency

The conventional wing aerodynamic efficiency is defined as:

$$\frac{L}{D} \tag{9}$$

For the CFJ wing, the ratio above still represents the pure aerodynamic relationship between lift and drag. However since CFJ active flow control consumes energy, the ratio above is modified to take into account the energy consumption of the pump. The formulation of the corrected aerodynamic efficiency for CFJ wings is:

$$(\frac{L}{D})_c = \frac{L}{D + \frac{P}{V_\infty}} \tag{10}$$

where V_∞ is the free stream velocity, P is the pumping power, and L and D are the lift and drag generated by the CFJ wing. The formulation above converts the power consumed by the CFJ into a force $\frac{P}{V_\infty}$ which is added to the aerodynamic drag D. If the pumping power is set to 0, this formulation returns to the aerodynamic efficiency of a conventional wing.

3 CFD Simulation Setup

3.1 CFD Code

The FASIP (Flow-Acoustics-Structure Interaction Package) CFD code is used to conduct the numerical simulation. The 3D Reynolds Averaged Navier-Stokes (RANS) equations with one-equation Spalart-Allmaras [19] turbulence model is used. A 5th order WENO scheme for the inviscid flux [20, 21, 22, 23, 24, 25] and a 4th order central differencing for the viscous terms [20, 24] are employed to discretize the Navier-Stokes equations. The low diffusion E-CUSP scheme used as the approximate Riemann solver suggested by Zha et al [21] is utilized with the WENO scheme to evaluate the inviscid fluxes. Implicit time marching method using Gauss-Seidel line relaxation is used to achieve a fast convergence rate [26]. Parallel computing is implemented to save wall clock simulation time [27].

Calculations are conducted at Mach number 0.10 and 0.15 to simulate the takeoff/landing and cruise conditions respectively. The Reynolds number based on the chord of the wing, is 1.8×10^6 and 2.6×10^6 respectively. The RANS solver is validated for CFJ airfoil simulation [9, 12, 17, 18].

3.2 Boundary Conditions

The 3rd order accuracy no slip condition is enforced on the solid surface with the wall treatment suggested in [28] to achieve the flux conservation on the wall, except at the wing tip where wall functions are used to reduce the mesh size. Total pressure, total temperature and flow angles are specified as the inlet boundary conditions for the upstream portion of the farfield boundary and inside the injection cavity. Constant static pressure is used for the downstream portion of the farfield boundary and inside the suction cavity. The symmetry boundary condition is used on the center plane of the wing so that only half of the wing needs to be simulated to save CPU resource.

To achieve zero net mass flux with the CFJ flow control, the mass flow exiting the injection slot must be equal to the mass flow entering the suction slot. Additionally, the jet strength must be controlled in order to reach the prescribed C_μ. The prescribed C_μ is achieved by adjusting the injection cavity total pressure. Total temperature is assumed constant during this process. The injection and suction mass flow are matched by adjusting the suction cavity static pressure. The process is iterated throughout the simulation until the specified momentum coefficient is reached and the injection and suction mass flow match within the tolerance of 1%.

3.3 Mesh

The mesh of the NACA 6415 baseline wing with no CFJ, shown in Fig. 4, is constructed using the O-mesh topology in order to achieve high quality around the wing. 160 points are placed around the wing partitioned equally between the suction and the pressure side, 80 points in the direction normal to the wing, 60 points in the spanwise direction. An O-mesh topology is also used for the wing tip. The total mesh size is 1.7 millions points, split into 34 blocks for the parallel computation. The far field boundary is located 30 chords away from the wing. The first grid point on the wing surface is placed at $y^+ \approx 1$ except on the wing tip wall where $y^+ \approx 50$ is used with the wall function boundary condition to reduce the mesh size.

The typical NACA 6415 CFJ wing mesh, shown in Fig.5, uses a similar mesh topology as the baseline wing. 280 points are placed around wing partitioned equally between the suction and the pressure side, 80

points in the direction normal to the wing, 40 points across the jet and 80 points in the spanwise direction. An O-mesh topology is also used for the wing tip. The total mesh size is 3.6 millions points, split into 111 blocks for the parallel computation. The far field boundary is located 50 chords away from the wing. The first grid point on the wing surface is placed at $y^+ \approx 1$ except on the wing tip wall where $y^+ \approx 50$ is used with the wall function boundary condition to reduce the mesh size.

4 Wing Configurations

In order to perform a trade study on CFJ wings, three CFJ airfoils are designed as shown in Fig. 2. Each CFJ airfoil is constructed from the baseline NACA airfoil by lowering the suction surface until an injection slot of 0.65% chord size and a suction slot of 1.30% chord size are formed on the modified suction surface (see Fig. 1). For instance, the top airfoil on Fig. 2 is built from a NACA 6415 airfoil by lowering the suction surface between 7% chord and 83.3% chord until the injection and suction slots are of the proper size. This airfoil is the original 15% thickness airfoil utilized in the wind tunnel experiments and previous 2D simulations [10, 11]. The middle airfoil has the injection and suction cavities redesigned. Furthermore, the injection slot is moved closer to the airfoil LE. The bottom airfoil is a 21% thickness airfoil that uses the same cavity design and slot position as the middle airfoil.

The geometry characteristics of the five CFJ wings designed in this trade study are summarized in Table 3. Each CFJ wing is constructed from a rectangular planform with no sweep and aspect ratio 20 (Design 1-4) or 10 (Design 5) by stacking the CFJ airfoils shown previously. The Design 1-2 use the top airfoil, the Design 3 uses the middle airfoil and the Design 4-5 use the bottom airfoil. Table 3 also gives the detailed slot size and location for each airfoil.

First, the simulations are performed on the Baseline 1 wing with no CFJ that uses the NACA 6415 airfoil and the Design 1 CFJ wing on the same planform in order to compare performance improvement. Then, each one of the Design 2-5 is simulated to show the influence of different slot location, airfoil thickness, implemented CFJ spanwise area from the root, and aspect ratio. For instance the influence of the spanwise area of the CFJ on the wing performance can be seen by comparing Design 1 (CFJ applied to 100% span) and Design 2 (CFJ applied only to 75% span) CFJ wings. The influence of the injection and suction cavity design and location is investigated by comparing the Design 1 (experiment cavities with injection slot located at 7% chord) and Design 3 (redesigned cavities with injection slot located at 2% chord) CFJ wings. The airfoil thickness is varied from 15% for the Design 3 to 21% for the Design 4. Finally the wing aspect ratio is reduced from 20 to 10 between the Design 4 and the Design 5.

Calculations are conducted at Mach number 0.15 with $0.04 \leq C_\mu \leq 0.08$ to simulate the cruise conditions of a general aviation airplane equipped with CFJ. Specifically, the cruise condition is $AoA = 5^\circ$ and C_μ of 0.04. The Design 4 CFJ wing is also simulated at Mach number 0.10 with $0.16 \leq C_\mu \leq 0.28$ to simulate the typical takeoff and landing conditions.

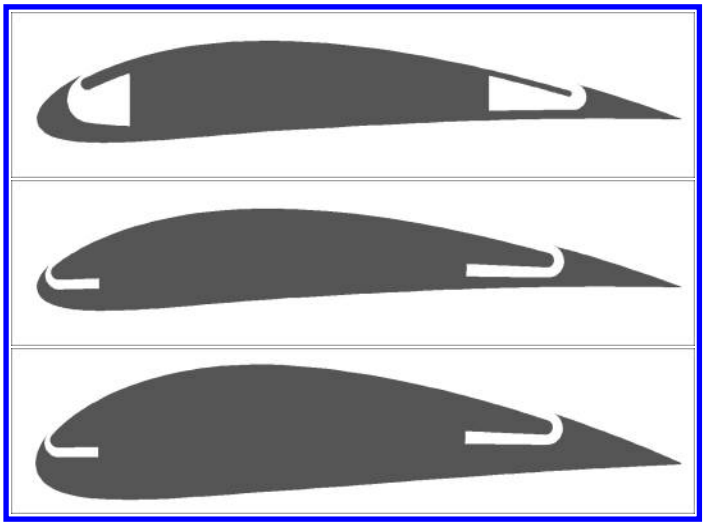

Figure 2: CFJ airfoils geometry.

	Baseline 1	Baseline 2	Baseline 3	Design 1	Design 2	Design 3	Design 4	Design 5
Planform	Rectangular	Rectangular	Rectangular	Rectangular	Rectangular	Rectangular	Rectangular	Rectangular
Aspect Ratio	20	20	10	20	20	20	20	10
Baseline airfoil	NACA 6415	NACA 6421	NACA 6421	NACA 6415	NACA 6415	NACA 6415	NACA 6421	NACA 6421
CFJ location (% span)	N/A	N/A	N/A	100	75	100	100	100
Injection slot location (% chord)	N/A	N/A	N/A	7.00	7.00	2.00	2.00	2.00
Suction slot location (% chord)	N/A	N/A	N/A	83.3	83.3	80.0	80.0	80.0
Injection slot size (% chord)	N/A	N/A	N/A	0.65	0.65	0.65	0.65	0.65
Suction slot size (% chord)	N/A	N/A	N/A	1.30	1.30	1.30	1.30	1.30
Cavities geometry	N/A	N/A	N/A	Experiment	Experiment	Redesigned	Redesigned	Redisigned

Figure 3: CFJ wings geometry.

5 Results

The trade study is to lay a foundation for the design of a general aviation electric airplane with 4 passengers and a range of about 300nm [16]. The cruise condition is $AoA = 5°$ and $C_\mu = 0.04$. The takeoff condition is $AoA = 25°$ and C_μ=0.20.

5.1 Design 1 CFJ Wing

The Design 1 CFJ wing is used as the first iteration of this trade study. The CFJ wing geometric characteristics are shown in Table 3. Fig. 6 shows the Design 1 CFJ wing surface pressure contours at AoA 15.0° and 25.0° with $C_\mu = 0.08$. At $AoA = 15.0°$ the main flow and the jet are fully attached. At AoA= 25.0°, a small flow separation appears at the wing TE. The flow is attached at the wing tip due to the lower local lift loading.

The Mach contours at 0%, 50%, and 99% span are plotted in Fig. 7 under the same flow conditions. The higher AoA feature a stagnation point located more downstream on the pressure side of the wing with a stronger LE acceleration. The small flow separation appears clearly with a recirculation located just upstream of the suction slot. Both AoAs plots show a much lower LE flow acceleration at 99% span hence a lower LE suction effect. This results in a lower jet velocity in the wing tip region even though the injection cavity pressure is constant. The close up view at the injection and suction cavities in Fig. 8 shows a jet Mach number about 0.4 at mid-span, AoA 15.0° and $C_\mu = 0.08$. The flow is separated in the suction cavity due to the large area expansion, which will be redesigned later.

Fig. 9 shows the chordwise distributions of the pressure coefficient and isentropic Mach number for the Baseline 1 wing at different span. The loading, visualized on the Cp and the isentropic Mach number plots, is similar for the inner 75% span of the wing. For the outer 25% span the loading is gradually decreased due to the wing tip effect. The same behavior is observed for the Design 1 CFJ wing as shown in Fig. 10. The spikes on the pressure distribution and isentropic Mach number are due to the injection and suction slots. The CFJ greatly augment the circulation due to an increased flow velocity on the suction surface as shown on the isentropic Mach number plots. Furthermore, comparing Fig. 9 with Fig. 10, the CFJ airfoil has a significantly higher suction peak near the LE than the baseline airfoil as demonstrated in the Cp plots. The combination of those effects increase the lift and lower the pressure drag of the airfoil. The maximum -Cp is 6.2 for the CFJ wing, an increase of roughly 50% over that of the Baseline 1 wing. Similarly the maximum isentropic Mach number of the CFJ wing is 0.41, an increase of roughly 20% over that of the baseline wing.

The forces, moment and power consumption versus AoA for the Design 1 CFJ wing are shown in Fig. 11. As aforementioned, the CFJ wing lift coefficient is significantly increased and reaches $C_{LMAX} = 2.3$ at $AoA = 25.0^\circ$ and $C_\mu = 0.08$, an increase of 41% over the Baseline 1 wing. The drag is only slightly increased at the mid-range AoA from 5° to 15°. At the higher C_μ value of 0.08, the drag is lower than the baseline at $AoA < 5^\circ$ and $AoA > 20^\circ$. The maximum aerodynamic L/D reaches the value of 62 at $AoA = 0.0^\circ$ and $C_\mu = 0.08$. The CFJ increases the pitch down moment due to higher lift. Unlike the baseline wing, the CFJ wing moment is fairly flat at low AoA and increases near the stall AoA. The power coefficient decreases with the increase of AoA until the near stall. When the flow separation occurs, the power coefficient is significantly increased due to the high total pressure loss shown by the ratio of total pressure at injection and suction in Fig. 12. The minimum power coefficient is small, as shown in Fig. 11, and reaches 0.006 at $C_\mu = 0.04$. A higher C_μ increases the power coefficient. The corrected aerodynamic efficiency (L/D)c reaches a maximum value of 23.2 at $AoA = 5.0^\circ$ and $C_\mu = 0.04$. This value is lower than the peak L/D of 33 achieved by the baseline wing, but is achieved for a lift coefficient almost twice higher, as shown in the (L/D)c vs AoA plot.

For a fixed C_μ, the power consumption depends mostly on the mass flow and total pressure ratio between the injection and suction cavities (see Eq. (7)). On the range of AoA studied, the mass flow is mostly constant, thereby, the changes in the pressure ratio are the main driver of the power consumption changes. Consequently, the behavior of the pressure ratio, shown in Fig. 12, determines the power coefficient given in Fig. 11. The total pressure ratio is only about 1.01 at $AoA = 10.0^\circ$ and $C_\mu = 0.04$. Fig. 13 shows the total pressure ratio between the injection cavity and the free stream. This pressure ratio indicates that the wing structure load due to the pressure difference inside and outside of the wing is very small. The ratio decreases with an increasing AoA due to the stronger LE suction. When the AoA is high enough, a C_μ in the range 0.04-0.06 achieves a pressure ratio lower than one, which means that the total pressure inside the injection cavity is lower than that of the free stream total pressure. Again, the difference is in the order of a few percent and the load is very small.

Fig. 14 shows a zoomed view of the static pressure contours in the vicinity of the injection region. The airfoil is in cruise condition at $AoA = 5.0^\circ$ and $C_\mu = 0.04$. The static pressure at the injection slot is not uniform due to the flow turning. The inner portion of the injection pressure is as low as 95% of the free stream pressure. The injection cavity pressure away from the injection slot is only about 2% above the free stream pressure and shows again that the mechanical stress resulting from the pressure difference between inside and outside of the wing is low.

5.2 CFJ Spanwise Area

The Design 2 CFJ wing has the CFJ area covering 75% of the inner span. Everything else remains the same as the previous design. The wing surface pressure contours is shown in Fig. 15. Unlike the Design 1 CFJ wing, the flow is attached up to $AoA = 25.0^\circ$ and $C_\mu = 0.08$. This is because the jet is distributed on the inner 75% span only and hence it is stronger than for a jet distributed on the full span for a same C_μ. The outer 25% span of the wing is also attached due to the lower local loading.

The forces, moment and power consumption versus AoA for the Design 2 CFJ wing are shown in Fig. 16. When compared with the Design 1 CFJ wing, the stronger jet of the Design 2 CFJ wing yield a higher stall AoA, a slightly lower drag coefficient and a higher power coefficient. The higher power coefficient is due to the reduced injection area that causes more total pressure loss. The moment coefficient is similar for both wings. The moment increase near the stall AoA is not significant with the Design 2 CFJ wing. Overall, the L/D of the Design 2 is slightly higher than that of the previous design at same AoA and C_μ. However the (L/D)c is a little lower due to the increase in power consumption. For the cruise condition at $AoA = 5.0°$ and $C_\mu = 0.04$, the L/D and (L/D)c reach 34.2 and 22.5 respectively, with a cruise C_L of 1.16.

5.3 CFJ Injection Location & Redesigned Cavities

The Design 3 CFJ wing injection slot is moved upstream to a 2% chord location to maximize the benefits from the LE low suction pressure effect on the jet power consumption. Furthermore, the injection and suction cavities are modified to reduces the duct diffusion and avoids the flow separation as shown in Fig. 17. Everything else remains the same as the Design 1 CFJ wing.

The resulting wing performance changes are shown in Fig. 18. The lift and moment coefficients are virtually unaffected by the design modification at the exception of a slightly lower stall AoA at $C_\mu = 0.08$. On the contrary, the drag and power coefficients are both lower. A Pc reduction of about 45% is achieved for $C_\mu = 0.08$. However, this power reduction decreases with reduced C_μ. At $C_\mu = 0.04$, little power reduction is observed. The lower power coefficient and lower drag yield a significantly higher L/D and $(L/D)_c$. For instance, during cruise at $AoA = 5.0°$ and $C_\mu = 0.04$, the cruise L/D and (L/D)c are 38.5 and 26.8 respectively. The cruise C_L is virtually unchanged. The peak efficiency has (L/D)c=26.8 and $C_L = 1.18$.

5.4 Airfoil Thickness

The Design 4 CFJ wing is constructed with the thicker NACA 6421 CFJ airfoil with everything else the same as Design 3, including the injection and suction cavity geometries and the slots locations. The reflected wing performance changes compared with the thick baseline 2 airfoil are shown in Fig. 19. The lift coefficient is significantly increased at low and medium AoA because a thicker airfoil increases the circulation if the flow is not separated. However, the stall AoA is slightly decreased and hence the CFJ wing maximum C_L is similar ($C_\mu = 0.08$) or slightly lower ($C_\mu = 0.04 - 0.06$) compared with that of Design 3. The drag coefficient is similar to that of the thinner CFJ wing. The pitch down moment is slightly increased. The power consumption of the thicker CFJ wing is slightly increased, and the (L/D)c is slightly decreased.

For the cruise condition at $AoA = 5.0°$ and $C_\mu = 0.04$, the L/D and (L/D)c are 38.8 and 25.2 respectively. The cruise C_L is increased by 5% and reaches 1.22. The peak efficiency point has (L/D)c=25.3 and $C_L = 1.44$. That is when the thickness is increased from 15% to 21%, the peak efficiency has a drop of 5.5%, but the corresponding lift coefficient is increased by 22%.

Fig. 19 also indicates that the Baseline 2 wing with no CFJ suffers a significant L/D loss due to the increased thickness with increased drag coefficient, whereas the thick CFJ airfoil only has the (L/D)c slightly reduced. Thereby, a CFJ wing can be designed to be very thick with little aerodynamic and energy expenditure penalties. Such a wing would benefit from important structural advantages in term of reduced weight, increased strength and inner volume.

5.5 Aspect Ratio

To study the effect of the aspect ratio, the Design 5 CFJ wing aspect ratio is decreased from 20 to 10. Everything else remains the same as the Design 4 CFJ wing. The reflected wing performance changes are shown in Fig. 20. The lower aspect ratio CFJ wing is more affected by the wing tip downwash, which

reduces the lift at same AoA and C_μ. In addition, the total drag is significantly increased due to the higher lift induced drag. Consequently the L/D ratio is significantly reduced when compared with the aspect ratio 20 wing. However, the aerodynamic L/D remains much higher than that of the Baseline 3 wing, which also features an aspect ratio of 10 with no CFJ (see Table 3). The stall AoA is increased due to the lower wing loading. Overall, the maximum lift coefficient is similar for $C_\mu = 0.04$ and $C_\mu = 0.06$ and even slightly increased for $C_\mu = 0.08$. The moment and power coefficients are virtually unaffected by the aspect ratio. For the cruise condition at $AoA = 5.0°$ and $C_\mu = 0.04$, the L/D and (L/D)c are 23.7 and 17.2 respectively, a significant reduction when compared with the aspect ratio 20 of the Design 4 CFJ wing.

5.6 High Lift at Takeoff/Landing

The Design 4 CFJ wing with 21% thickness airfoil thickness and aspect ratio of 20 is simulated at a high AoAs (20° - 40°), and high C_μ (0.16 - 0.28). A Mach number of 0.1 is used to simulate the takeoff/landing conditions. The resulting surface isentropic Mach number contours are shown in Fig. 21. A Large flow acceleration is located at the airfoil LE and suction surface, which is responsible for the very high lift and low pressure drag. The flow is fully attached for this case at $AoA = 25.0°$ and $C_\mu = 0.20$.

The wing performance are shown on Fig. 22. At $C_\mu = 0.28$ the flow is attached up to $AoA = 40.0°$ and the maximum C_L reaches a very high value of 4.7. The drag coefficient between $AoA = 20.0°$ and $AoA = 25.0°$ is similar for all the momentum coefficients. However at higher AoA, a higher C_μ yield a higher drag coefficient mostly because of the greater lift induced drag. The moment coefficient remains contained between -0.2 and -0.3. The power coefficient is significantly increased because of the high C_μ. However the actual power consumption increase, which depends on the cube of the free stream velocity as indicated by Eqs. 7 and 8, is reasonable. Even with a very high C_L, the CFJ wing still achieves a good L/D and (L/D)c. For example, at $AoA = 25.0°$ and $C_\mu = 0.20$, the lift coefficient is a 3.5 with a corresponding L/D and (L/D)c of 16.3 and 10.4 respectively. At this condition, the wing still has a wide stall margin of about 10.0°.

Even for the very large AoA studied here, the power coefficient still decreases with the increase of AoA until the near stall. When the flow separation occurs, the power coefficient is drastically increased due to the high total pressure loss as shown in Fig. 23. This behavior is similar to what we have seen in Fig. 12 for the cruise condition, albeit with higher value of AoA and C_μ. The total pressure ratio is increased when compared to cruise, but remains contained to less than 1.04 for a typical takeoff and landing condition.

Fig. 24 shows a close up view of the static pressure contours in the vicinity of the injection region. The CFJ wing is at takeoff/landing condition at $AoA = 25.0°$ and $C_\mu = 0.20$. Similarly to the cruise condition shown in Fig. 14, most of the injection cavity pressure away from the injection slot is only about 2% above the free stream pressure and hence the mechanical stress resulting from the pressure difference between inside and outside of the airfoil is low.

5.7 Recapitulation of CFJ Wing Performance

In the previous sections, the CFJ wing is demonstrated to have very good aerodynamic efficiency $(L/D)_c$ with substantially higher lift coefficient than conventional airfoil. This section hence summarize the distinguishable characteristics of the CFJ wing to demonstrate the $(L/D)_c$ vs C_L in Fig. 25. The plots are organized to ease the comparison among the CFJ wing designs.

Design 1 and 2 performed similarly, with a slight increase in efficiency for the Design 1 airfoil. Hence applying CFJ on the 75% inner potion of the wing surface did not provide a significant change in performance. Design 3 however performed much better due to the removal of the separation in the suction cavity and the redesign of the injection cavity. When the CFJ wing thickness is increased from 15% to 21%, the peak efficiency of the thick baseline wing with no CFJ drops significantly from 31.6 to 26.8 by 15%, which is expected. However, the CFJ wing peak efficiency is only dropped by 5.5% and the corresponding CFJ wing

lift coefficient is increased by 22%. The Design 4 CFJ wing with 21% thickness at $C_\mu = 0.04$ reaches a maximum efficiency very close to the baseline 2 wing. The thick baseline 2 wing achieves the peak L/D of 26.8 at $C_L = 0.68$, whereas the thick CFJ 4 wing achieves the peak $(L/D)_c$ of 25.3 at $C_L = 1.44$. In other words, the aerodynamic efficiency drops by about 5.5%, but the lift coefficient is increased by 110%. It is believed that the CFJ airfoil can achieve even better aerodynamic efficiency with a systematic optimization.

Such a drastic increase of lift coefficient with excellent aerodynamic efficiency will allow the aircraft to substantially increase wing loading and reduce the size and weight. Such an extraordinary wing performance will bring a radically different design philosophy to revolutionize the future aircraft design. The high wing loading general aviation electric aircraft (GA-EA [16]) conceptually designed by Lefebvre and Zha using CFJ wing benefits from this new technology. The CFJ GA-EA achieves the wing loading about 3 times higher than conventional design. In principle, the CFJ GA-EA may achieve a range 3 times longer than a same size conventional GA airplane due to bring much more battery, or for the same range, the CFJ GA-EA can have the wing area reduced by 67%.

When lowering the aspect ratio from 20 to 10, both the baseline and the CFJ wing efficiency is significantly reduced due to the increased in lift-induced drag. However, the maximum C_L of the CFJ wing is slightly higher than that of the wing with aspect ratio of 20.

The Design 4 CFJ wing performance at takeoff/landing configuration is also remarkable as described in section 5.6. Fig. 25 also clearly exhibits a peak efficiency line vs C_L for both the cruise and takeoff/landing condition, which is constructed by joining the peak efficiency points of the different C_μ lines. A higher C_μ reaches a lower peak efficiency at a higher C_L. Thus, it is possible to chose a C_μ that maximizes the efficiency for a given C_L.

6 Conclusions

This article performs a trade study on 3D CFJ wings. The NACA 6415 CFJ airfoil is chosen for the first CFJ wing design due to the presence of 2D experimental and computational data. The CFJ spanwise location is varied from 75% span to 100% span, the injection and suction cavities are redesigned and the injection slot is moved from 7% chord to 2% chord. The airfoil thickness is varied from 15% to 21%. Finally, the wing aspect ratio is varied from 10 to 20. The ultimate goal of the trade study is to generate a CFJ wing with high cruise wing loading and aerodynamic efficiency, high maximum lift coefficient, low moment, and low power consumption. The calculations are performed at Mach number 0.10 and 0.15 to simulate the typical takeoff/landing and cruise velocity of a general aviation aircraft. The Reynold numbers based on the wing chord are 1.8×10^6 and 2.6×10^6 respectively.

The aerodynamic efficiency $(L/D)_c$ depends the wing lift, drag and CFJ pumping power coefficient. For the same injection momentum coefficient, the CFJ area covering 99% of the span has slightly higher aerodynamic efficiency than the one with 75% CFJ area. The latter has a little higher power coefficient since the smaller injection area suffers more loss. The internal duct of CFJ pumping is very important to determine the overall aerodynamic efficiency. A design with suction duct separation removed significantly increases the overall aerodynamic efficiency due to reduced pumping power coefficient. When the thickness is increased from 15% to 21%, the peak efficiency of the thick baseline wing with no CFJ drops significantly from 31.6 to 26.8 by 15%, which is expected. However, the peak CFJ wing aerodynamic efficiency drops only by 5.5%, but the corresponding lift coefficient at the peak efficiency point is increased by 22%.

The CFJ wing with a 21% thickness at cruise achieves a maximum L/D of 38.5 at a remarkably high C_L of 1.20 and C_μ of 0.04 . When the CFJ pump power P is taken into account, the corrected aerodynamic efficiency $L/(D + P/V_\infty)$ is 25.2. The takeoff/landing performance are also excellent with a maximum C_L of 4.7 achieved at C_μ of 0.28 and AoA of 40.0°. For takeoff/landing, the CFJ wing moment is lower than the conventional high lift system using flaps and hence smaller tail force is needed for trimming purpose. The 21% thickness CFJ wing is particular advantageous to have high aerodynamic efficiency and lift coefficient. It has a drop of peak aerodynamic efficiency of 5.5%, but has the lift coefficient increase by 110%. In addition,

it provides a significant structural advantage with increased strength, reduced weight and an increased inner volume.

Overall, this study demonstrates that the CFJ airfoil is not only very effective to drastically increase the maximum lift coefficient, but also able to achieve a high aerodynamic efficiency with ultra-high lift coefficient at cruise due to its low energy expenditure. The drastically increased lift coefficient with excellent aerodynamic efficiency at cruise will allow the aircraft to substantially increase wing loading and hence reduce the wing size and weight. Such an extraordinary wing performance could results in a radically different design philosophy and lead to revolutionary aircraft design, such as the high wing loading general aviation electric aircraft (GA-EA [16]) studied by Lefebvre and Zha.

7 Acknowledgment

The CFD simulation of this research is conducted at the Center for Computational Sciences of the University of Miami.

References

[1] N. Wood and J. Nielsen, "Circulation Control Airfoils-Past, Present, Future." AIAA Paper 85-0204, 1985.

[2] R. J. Englar, "Circulation Control Pneumatic Aerodynamics: Blown Force and Moment Augmentation and Modifications; Past, Present and Future." AIAA 2000-2541, June 2000.

[3] G. S. Jones, "Pneumatic Flap Performance for a 2D Circulation Control Airfoil, Stedy & Pulsed." *Applications of Circulation Control Technologies*, Chapter 7, p. 191-244, Vol. 214, Progress in Astronautics and Aeronautics, AIAA Book Series, Editors: Joslin, R. D. and Jones, G. S., 2006.

[4] R. Holman, Q. Gallas, B. Carroll, and L. Cattafesta, " Interaction of Adjacent Synthetic Jets in an Airfoil Separation Control Application." AIAA Paper 2003-3709, June 2003.

[5] G.-C. Zha and D. C. Paxton, "A Novel Flow Control Method for Airfoil Performance Enhancement Using Co-Flow Jet." *Applications of Circulation Control Technologies*, Chapter 10, p. 293-314, Vol. 214, Progress in Astronautics and Aeronautics, AIAA Book Series, Editors: Joslin, R. D. and Jones, G.S., 2006.

[6] G.-C. Zha, W. Gao, and C. Paxton, "Jet Effects on Co-Flow Jet Airfoil Performance," *AIAA Journal, No. 6,*, vol. 45, pp. 1222–1231, 2007.

[7] G.-C. Zha, C. Paxton, A. Conley, A. Wells, and B. Carroll, "Effect of Injection Slot Size on High Performance Co-Flow Jet Airfoil," *AIAA Journal of Aircraft*, vol. 43, 2006.

[8] G.-C. Zha, B. Carroll, C. Paxton, A. Conley, and A. Wells, "High Performance Airfoil with Co-Flow Jet Flow Control," *AIAA Journal*, vol. 45, 2007.

[9] Wang, B.-Y. and Haddoukessouni, B. and Levy, J. and Zha, G.-C., "Numerical Investigations of Injection Slot Size Effect on the Performance of Co-Flow Jet Airfoil," *Journal of Aircraft*, vol. 45, No. 6, pp. 2084–2091, 2008,.

[10] B. P. E. Dano, D. Kirk, and G.-C. Zha, "Experimental Investigation of Jet Mixing Mechanism of Co-Flow Jet Airfoil." AIAA-2010-4421, 5th AIAA Flow Control Conference, Chicago, IL, 28 Jun - 1 Jul 2010.

[11] B. P. E. Dano, G.-C. Zha, and M. Castillo, "Experimental Study of Co-Flow Jet Airfoil Performance Enhancement Using Micro Discreet Jets." AIAA Paper 2011-0941, 49th AIAA Aerospace Sciences Meeting, Orlando, FL, 4-7 January 2011.

[12] A. Lefebvre, B. Dano, M. D. Fronzo, W. B. Bartow, and G-C. Zha, "Performance of a Co-Flow Jet Airfoil with Variation of Mach Number," *AIAA paper 2013-490*, Jan 2013.

[13] A. Lefebvre, G-C. Zha, "Numerical Simulation of Pitching Airfoil Performance Enhancement Using Co-Flow Jet Flow Control," *AIAA paper 2013-2517*, June 2013.

[14] A. Lefebvre, G-C. Zha, "Co-Flow Jet Airfoil Trade Study Part I : Energy Consumption and Aerodynamic Performance," *AIAA paper 2014-2682*, June 2014.

[15] A. Lefebvre, G-C. Zha, "Co-Flow Jet Airfoil Trade Study Part II : Moment and Drag," *AIAA paper 2014-2683*, June 2014.

[16] A. Lefebvre and G-C. Zha, "Conceptual Design of an Electric Airplane Utilizing Co-Flow Jet Flow Control," *AIAA Paper 2015-0772, 53rd AIAA Aerospace Sciences Meeting*, Jan 2015.

[17] Wang, B. Y and Zha, G.-C. , "Detached-Eddy Simulation of a Co-Flow Jet Airfoil at High Angle of Attack." AIAA Journal of Aircraft, Vol. 48, No. 5, 2011.

[18] Im, H. , Zha, G.-C., and Dano, B. P. E., "Large Eddy Simulation of Coflow Jet Airfoil at High Angle of Attack." Journal of Fluids Engineering, Vol. 136 / 021101-1, Feb. 2014.

[19] P. Spalart and S. Allmaras, "A One-equation Turbulence Model for Aerodynamic Flows." AIAA-92-0439, 1992.

[20] Y.-Q. Shen and G.-C. Zha, "Large Eddy Simulation Using a New Set of Sixth Order Schemes for Compressible Viscous Terms ," *Journal of Computational Physics*, vol. 229, pp. 8296–8312, 2010.

[21] G.-C. Zha, Y. Shen, and B. Wang, "An improved low diffusion E-CUSP upwind scheme ," *Journal of Computer & Fluids*, vol. 48, pp. 214–220, 2011.

[22] Y.-Q. Shen and G.-Z. Zha , "Generalized finite compact difference scheme for shock/complex flowfield interaction," *Journal of Computational Physics*, vol. doi:10.1016/j.jcp.2011.01.039, 2011.

[23] Shen, Y.-Q. and Zha, G.-C. and Wang, B.-Y., " Improvement of Stability and Accuracy of Implicit WENO Scheme," *AIAA Journal*, vol. 47, No. 2, pp. 331–344, 2009.

[24] Shen, Y.-Q. and Zha, G.-C. and Chen, X.-Y., " High Order Conservative Differencing for Viscous Terms and the Application to Vortex-Induced Vibration Flows," *Journal of Computational Physics*, vol. 228(2), pp. 8283–8300, 2009.

[25] Shen, Y.-Q. and Zha, G.-C. , " Improvement of the WENO Scheme Smoothness Estimator," *International Journal for Numerical Methods in Fluids*, vol. DOI:10.1002/fld.2186, 2009.

[26] G.-C. Zha and E. Bilgen, "Numerical Study of Three-Dimensional Transonic Flows Using Unfactored Upwind-Relaxation Sweeping Algorithm," *Journal of Computational Physics*, vol. 125, pp. 425–433, 1996.

[27] B.-Y. Wang and G.-C. Zha, "A General Sub-Domain Boundary Mapping Procedure For Structured Grid CFD Parallel Computation," *AIAA Journal of Aerospace Computing, Information, and Communication*, vol. 5, No.11, pp. 2084–2091, 2008.

[28] Y.-Q. Shen, G.-C. Zha, and B.-Y. Wang, "Improvement of Stability and Accuracy of Implicit WENO Scheme ," *AIAA Journal*, vol. 47, pp. 331–344, 2009.

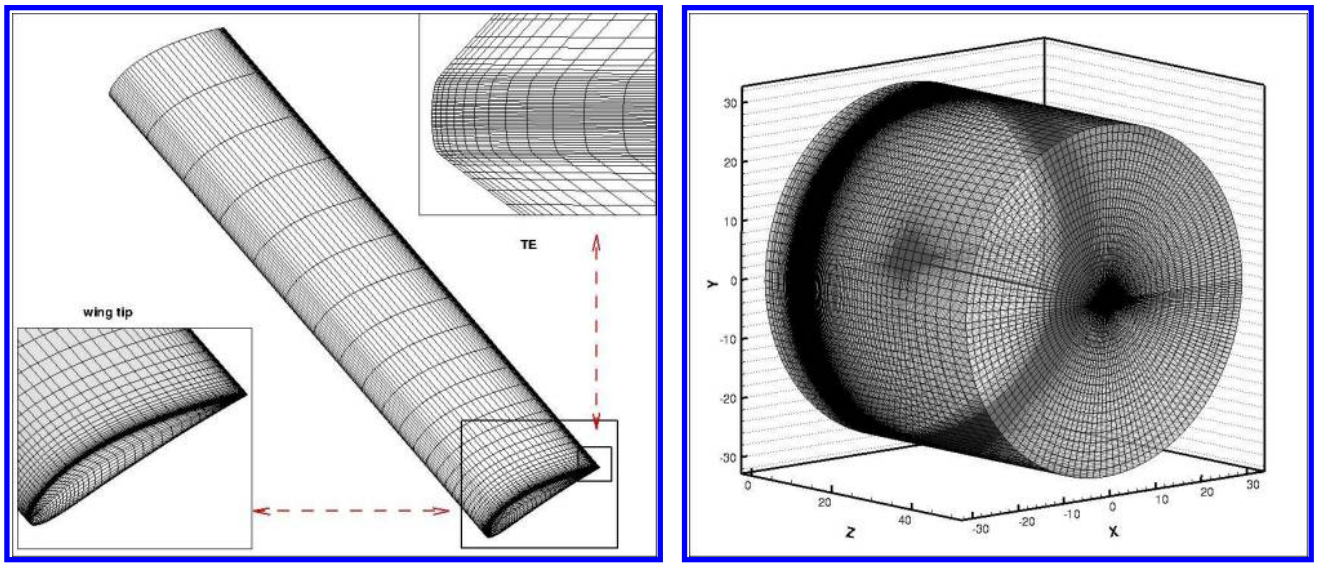

Figure 4: NACA 6415 baseline wing mesh topology. The surface mesh is displayed on the top plot and the outer mesh on the lower plot.

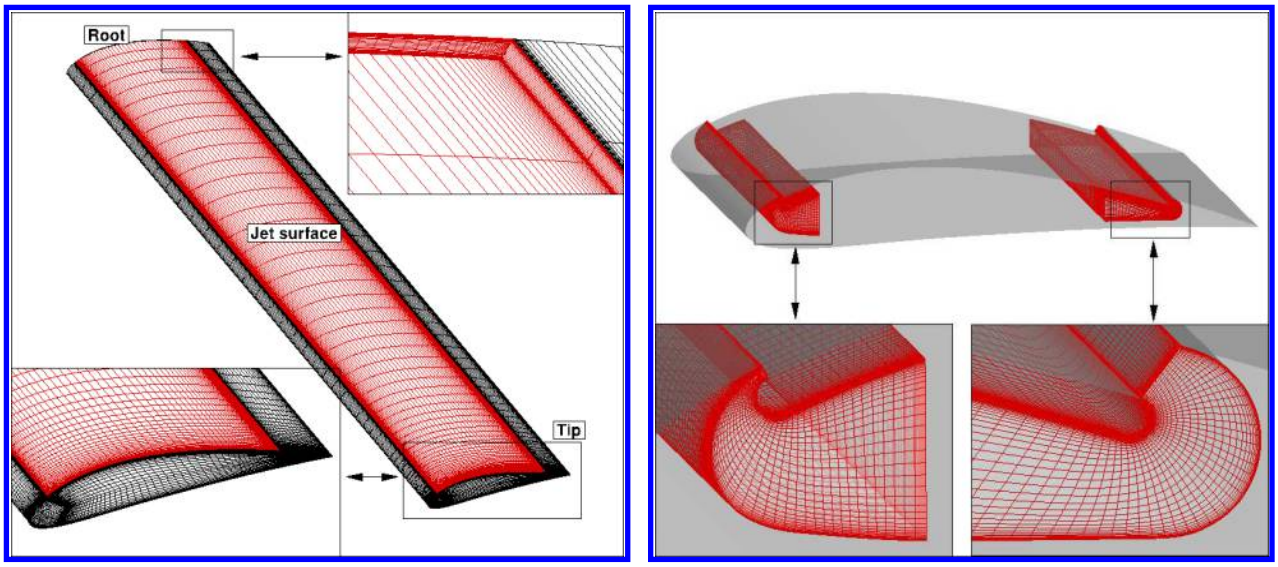

Figure 5: CFJ 6415 wing mesh topology. The surface mesh is displayed on the left plot and the injection and suction cavity mesh on the right plot.

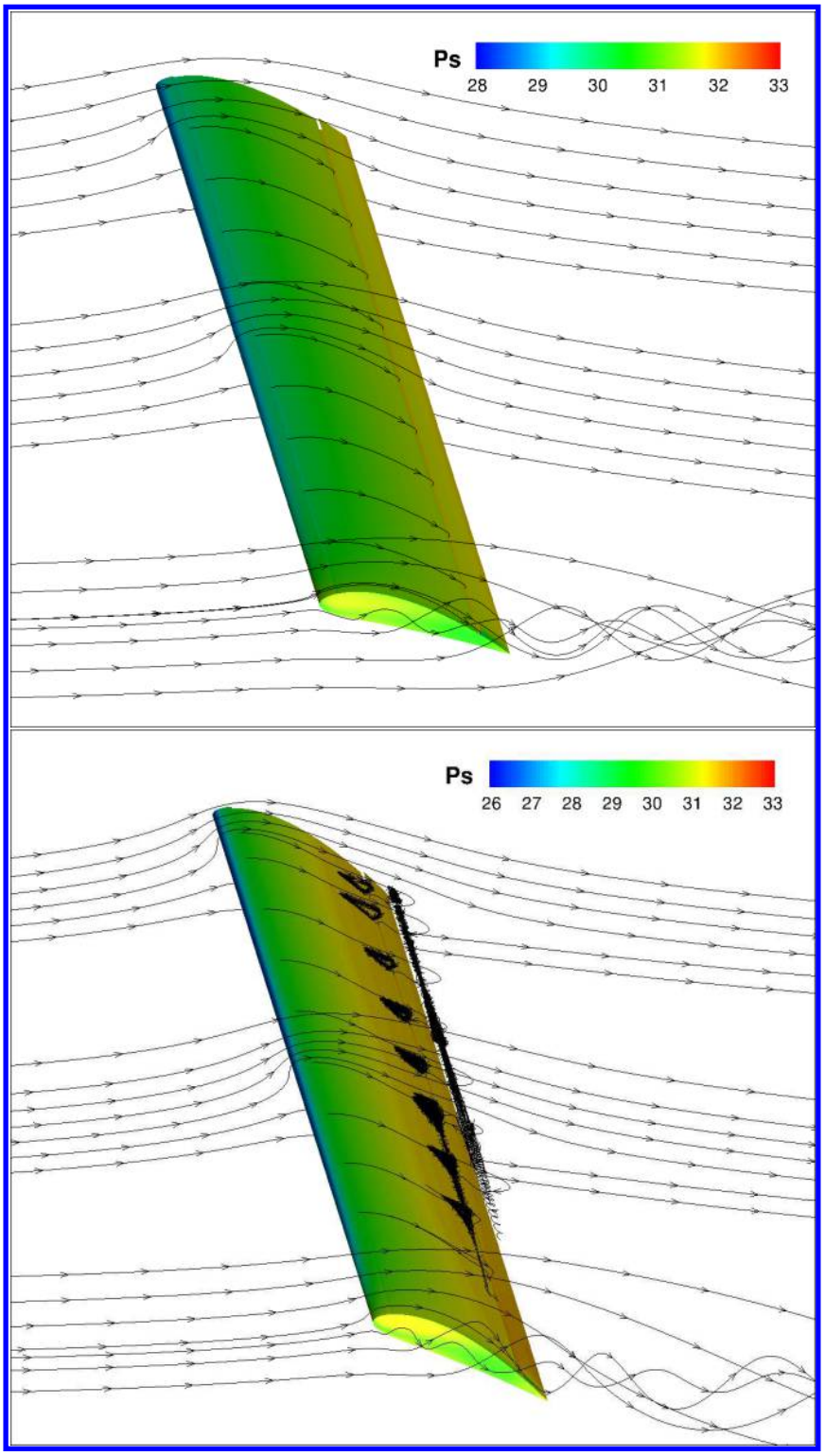

Figure 6: Surface pressure contours with streamlines for the Design 1 CFJ wing at $C_\mu = 0.08$. The AoA is 15° on the left and 25° on the right.

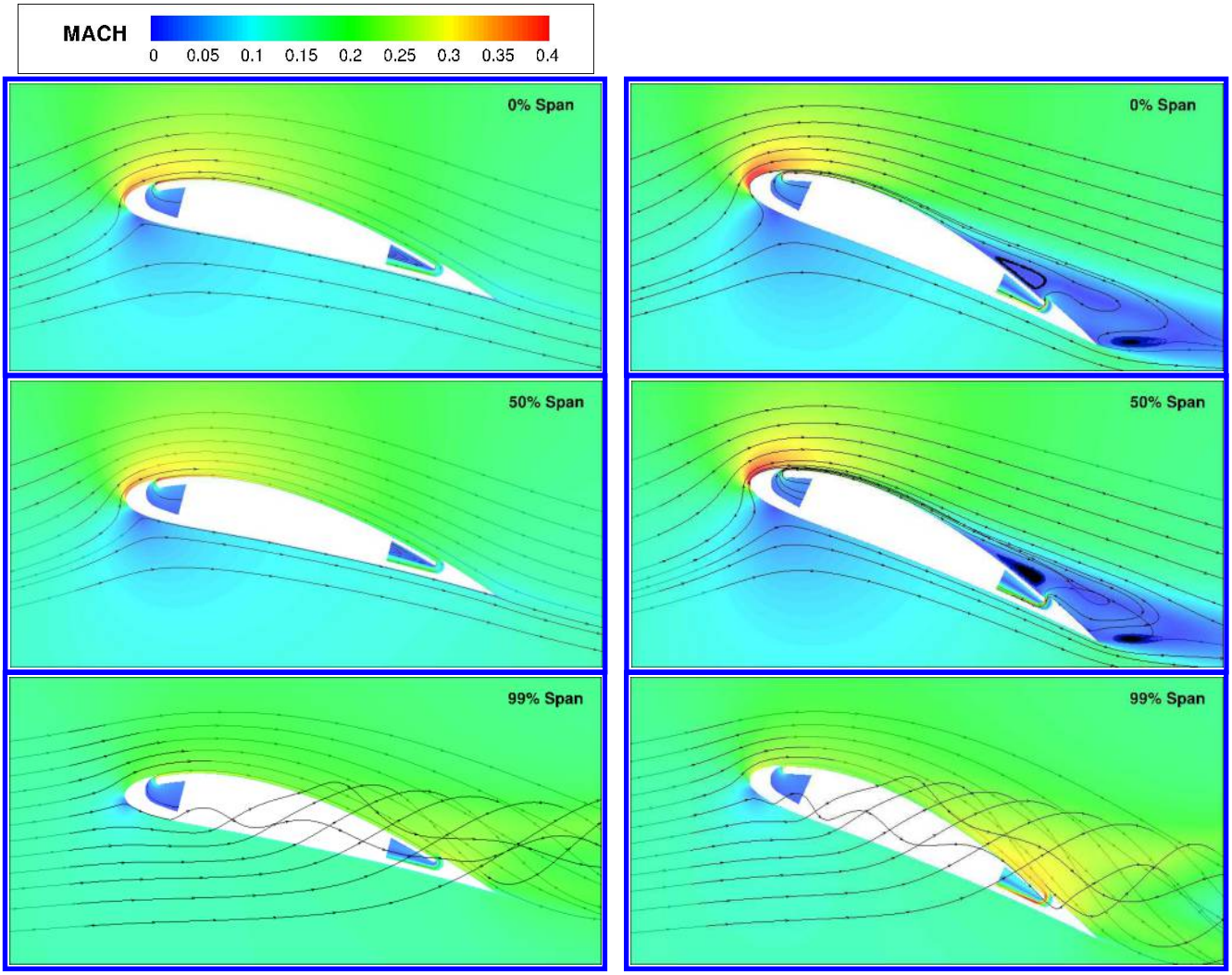

Figure 7: Mach contours with streamlines at 0%, 50% and 99% spanwise location for the Design 1 CFJ wing at $C_\mu = 0.08$. The AoA is 15° for the left plots and 25° for the right plots.

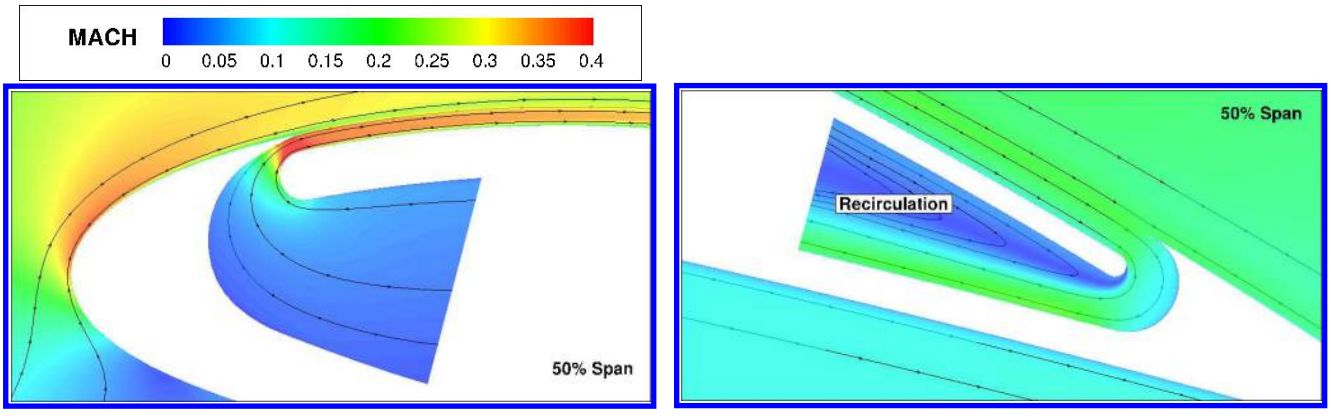

Figure 8: Close up view of the experimental injection and suction cavities for the Design 1 CFJ wing. Mach contours at 50% spanwise location, $C_\mu = 0.08$ and $AoA = 15°$.

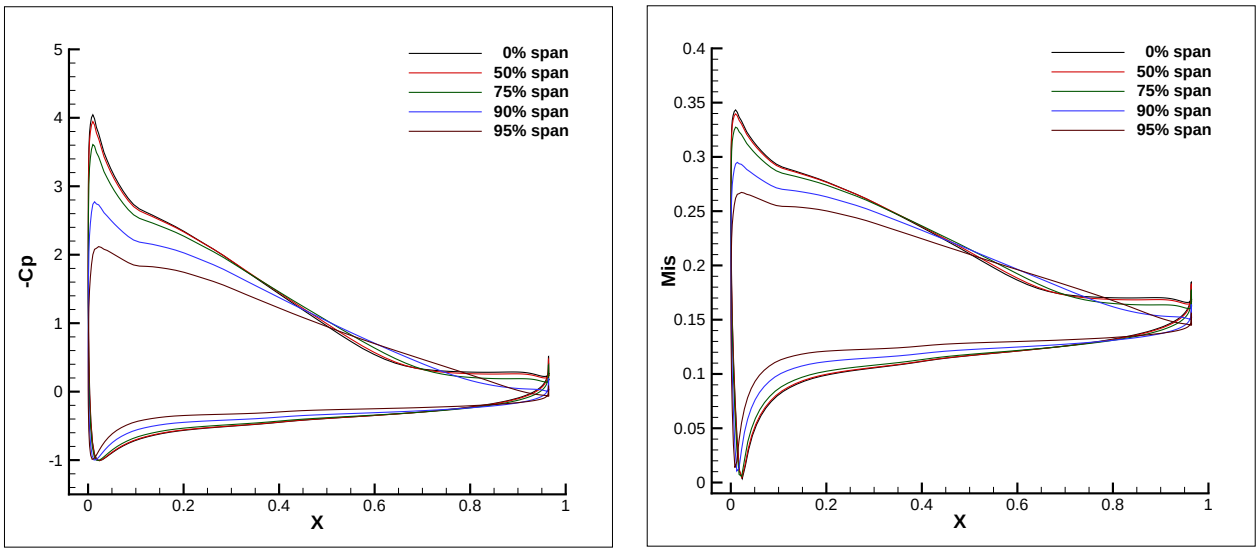

Figure 9: Pressure coefficient (left) and isentropic Mach number (right) at various spanwise location for the baseline NACA 6415 wing without CFJ at $AoA = 15°$.

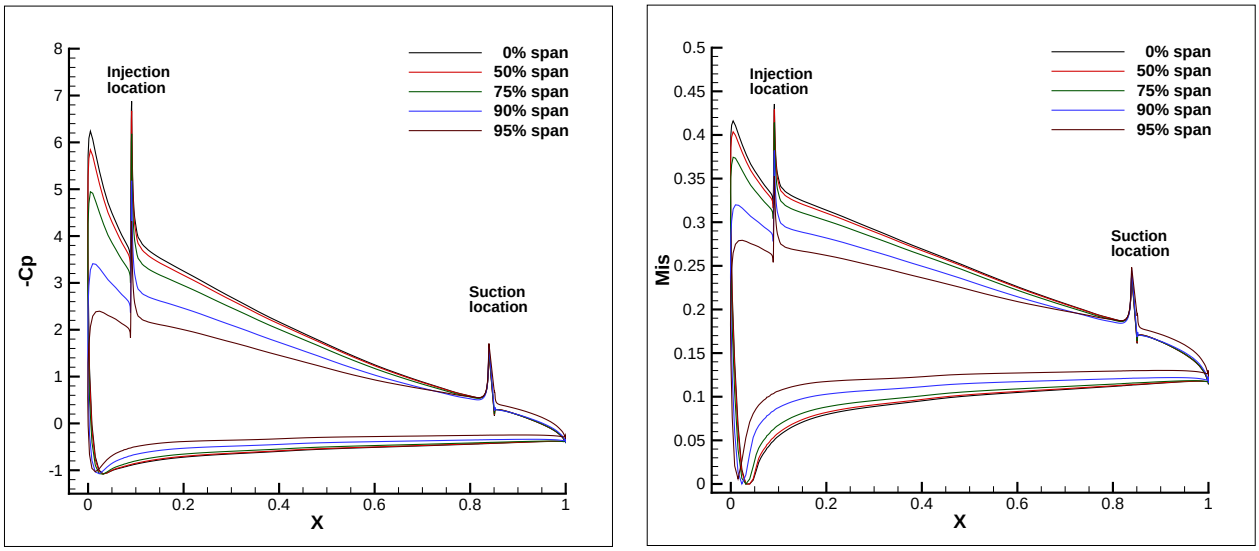

Figure 10: Pressure coefficient (left) and isentropic Mach number (right) at various spanwise location for the Design 1 CFJ wing at $AoA = 15°$ and $C_\mu = 0.08$.

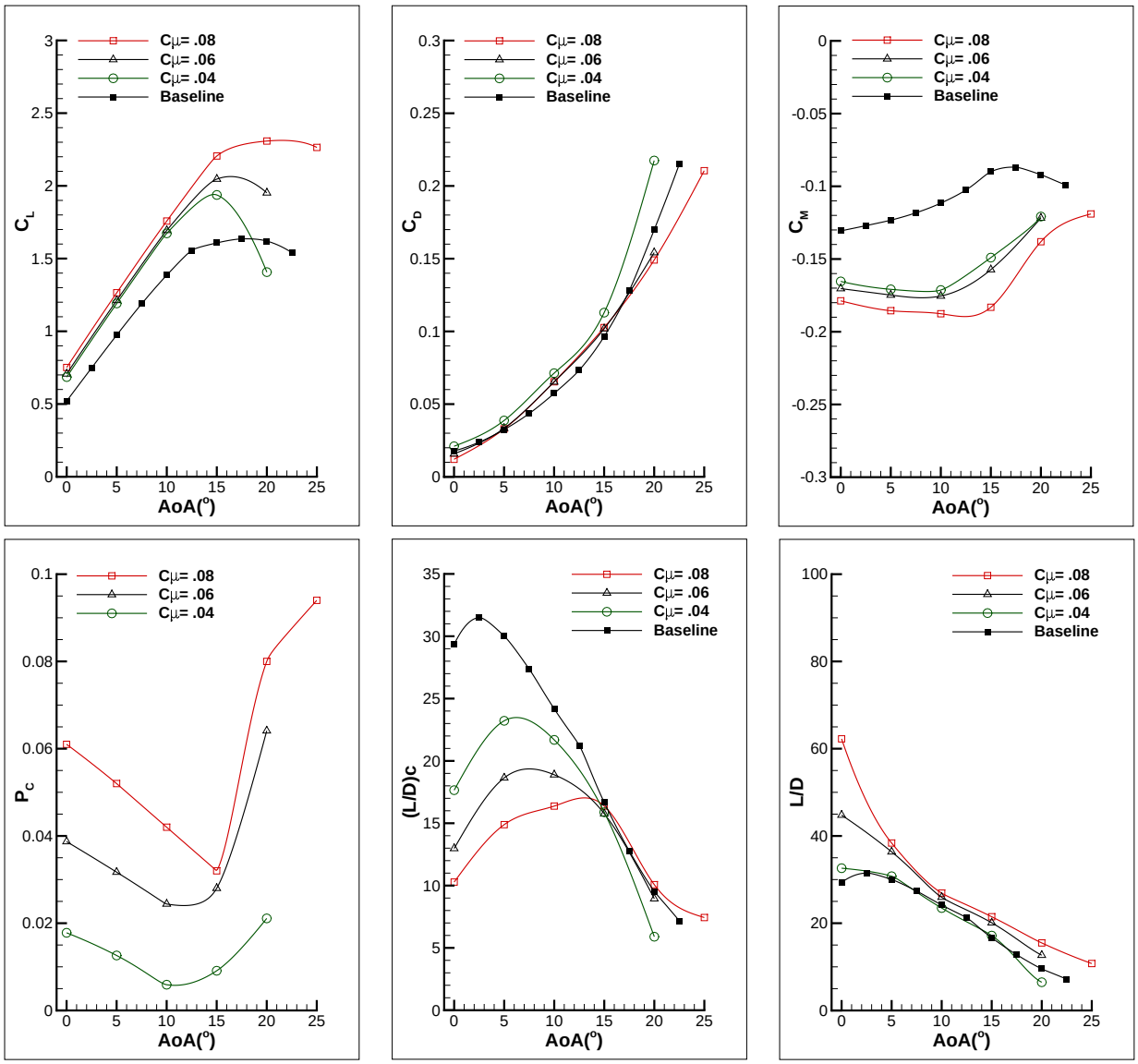

Figure 11: Forces, moment and energy expenditure versus AoA for the Design 1 CFJ wing. Simulations performed at M=0.15 and $0.04 \leq C_\mu \leq 0.08$.

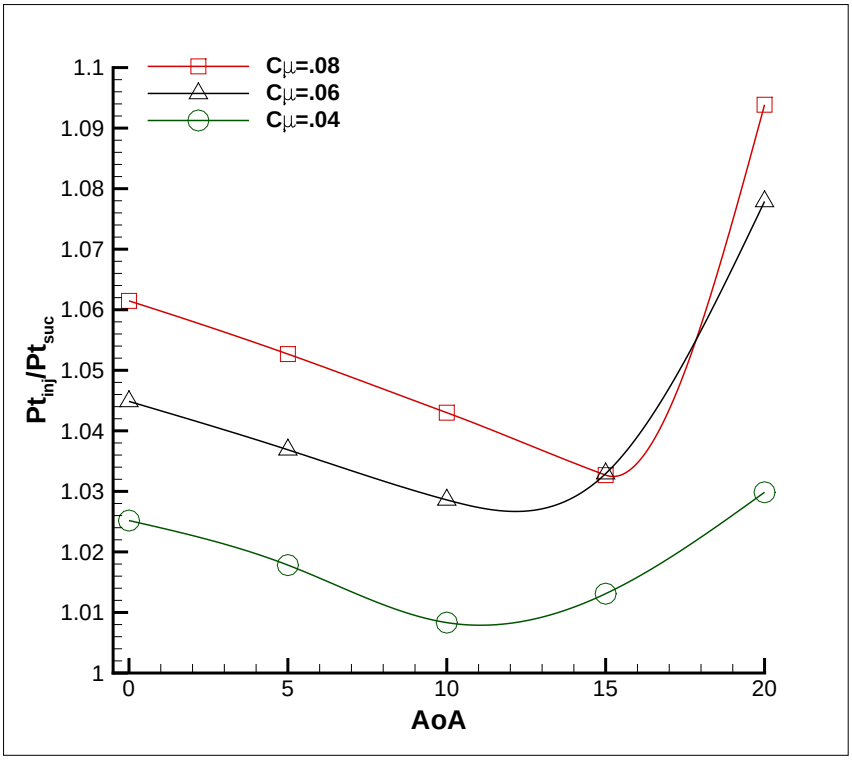

Figure 12: Mass-averaged total pressure ratio between the injection and suction cavities for the Design 1 CFJ wing.

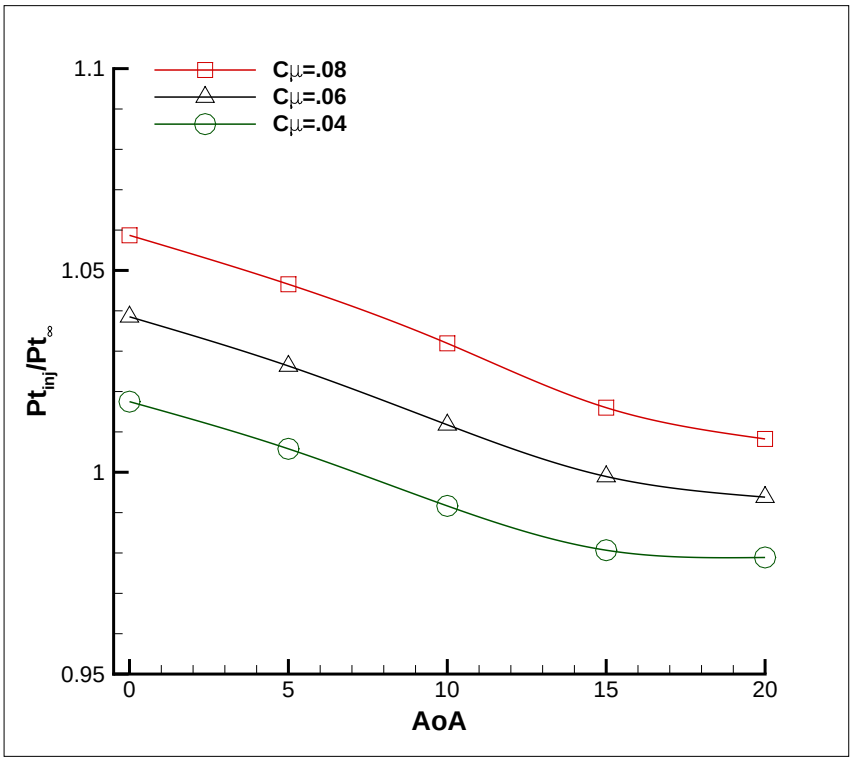

Figure 13: Mass-averaged total pressure ratio between the injection cavity and the free stream for the Design 1 CFJ wing .

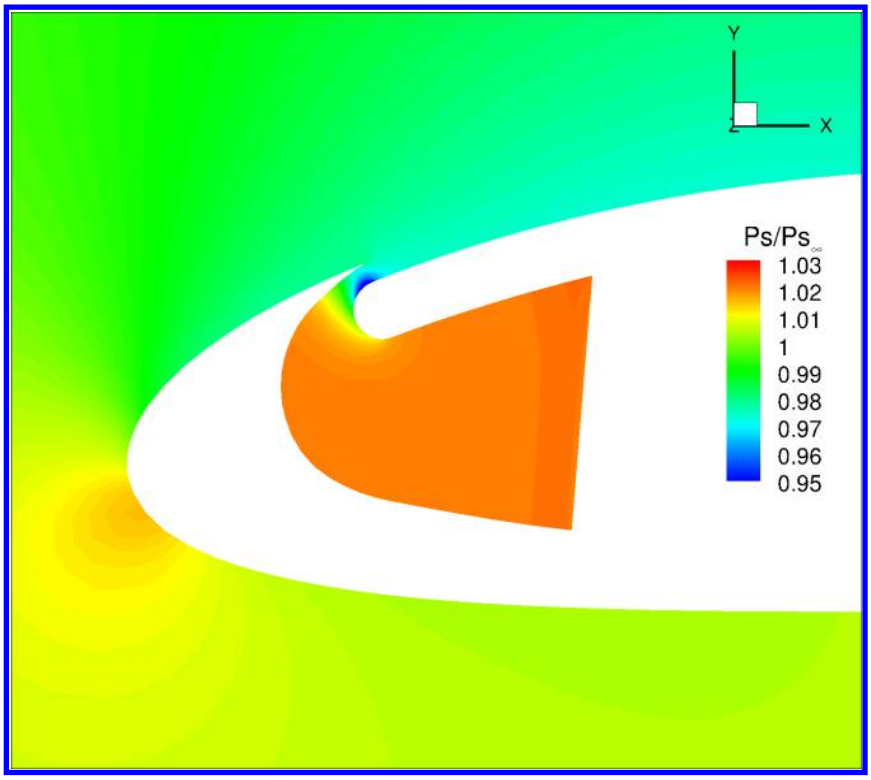

Figure 14: Static pressure contours at 50% spanwise location for the Design 1 CFJ wing. The CFJ wing is in cruise condition at $AoA = 5.0^{\circ}$ and $C_{\mu} = 0.04$. The normalized free stream static pressure is 1.00.

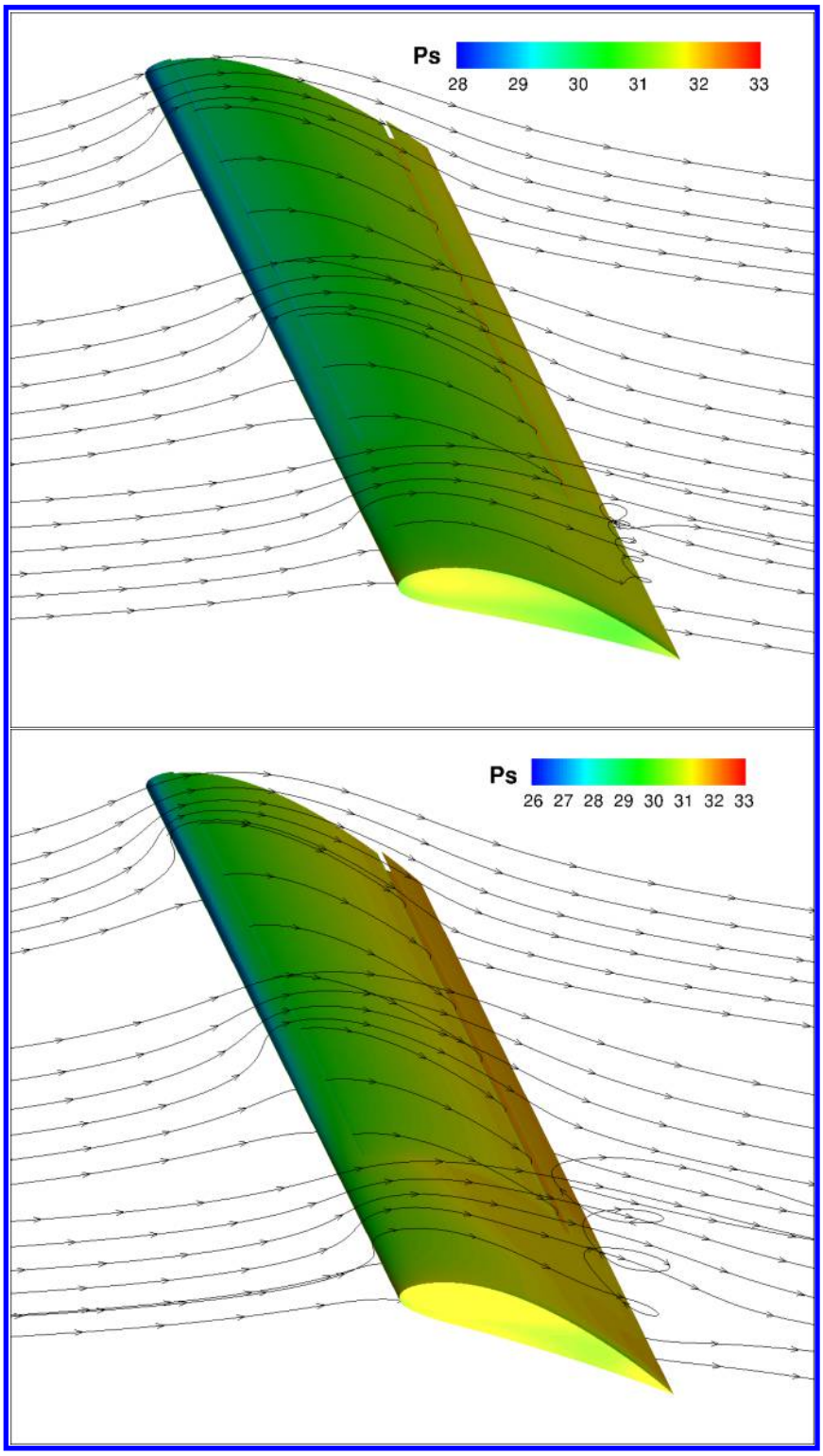

Figure 15: Surface pressure contours with streamlines for the Design 2 CFJ wing at $C_\mu = 0.08$. The top plot is at at AoA=15° and the bottom plot at AoA=25°.

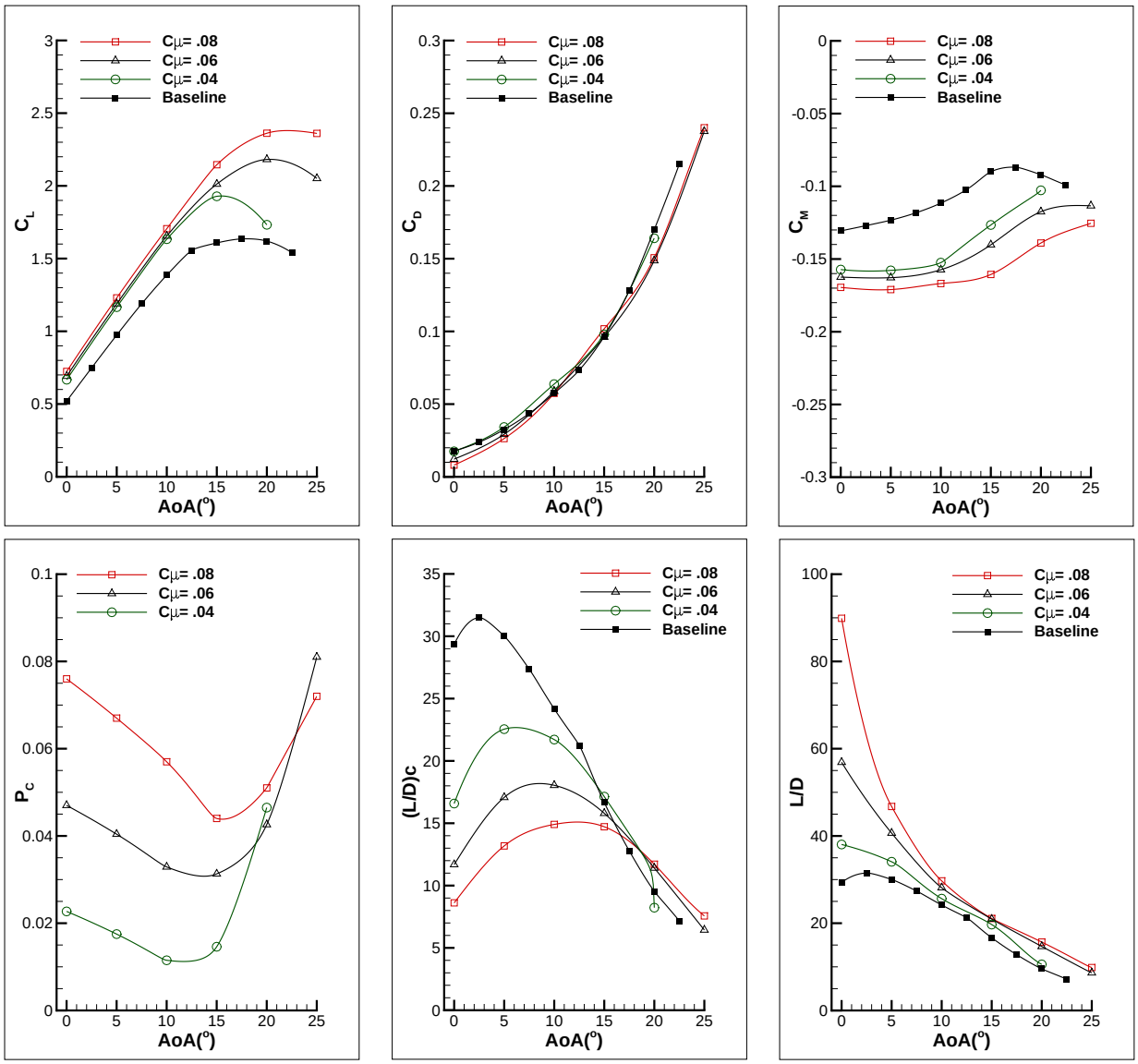

Figure 16: Forces, moment and energy expenditure versus AoA for the Design 2 CFJ wing. Simulations performed at M=0.15 and $0.04 \leq C_\mu \leq 0.08$.

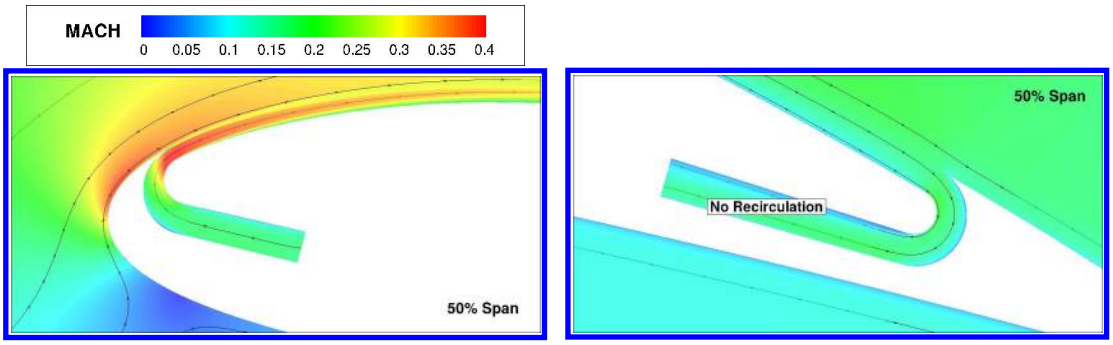

Figure 17: Mach contours with streamlines at 50% spanwise location for the Design 3 CFJ wing at $C_\mu = 0.08$ and $AoA = 15°$.

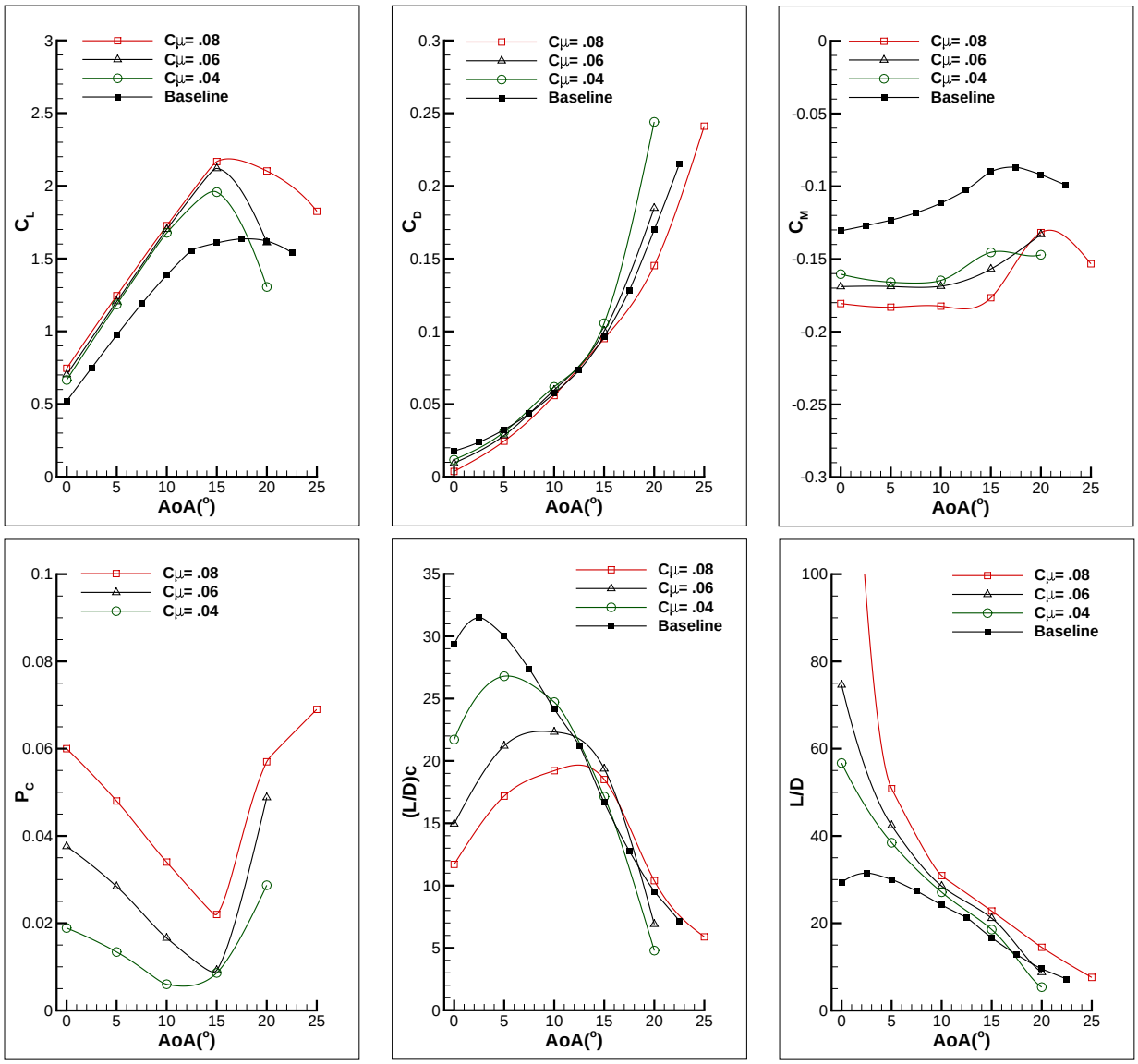

Figure 18: Forces, moment and energy expenditure versus AoA for the Design 3 CFJ wing. Simulations performed at M=0.15, $0.04 \leq C_\mu \leq 0.08$.

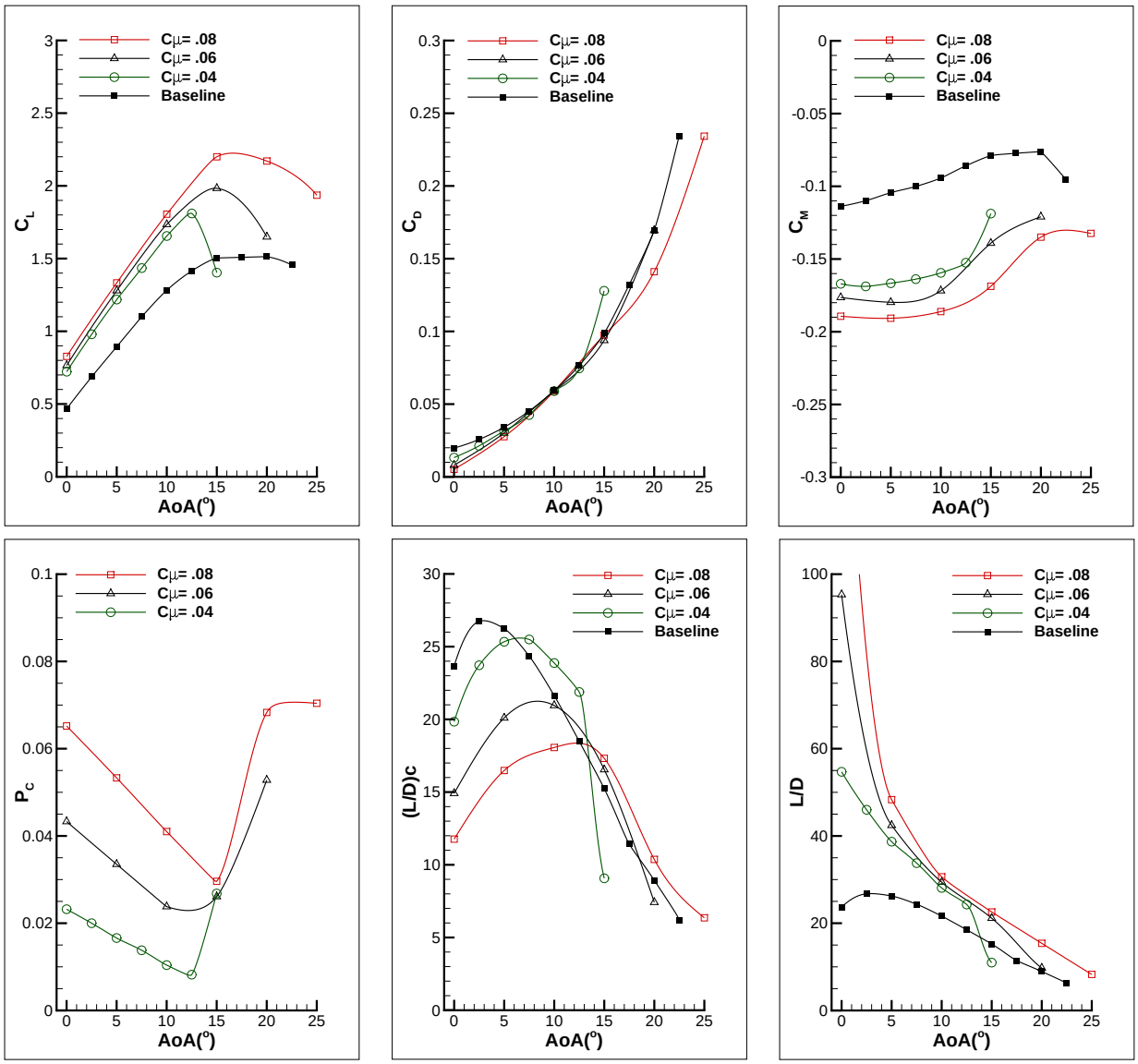

Figure 19: Forces, moment and energy expenditure versus AoA for the Design 4 CFJ wing compared with the baseline 2 airfoil. Simulations performed at M=0.15, $0.04 \leq C_\mu \leq 0.08$.

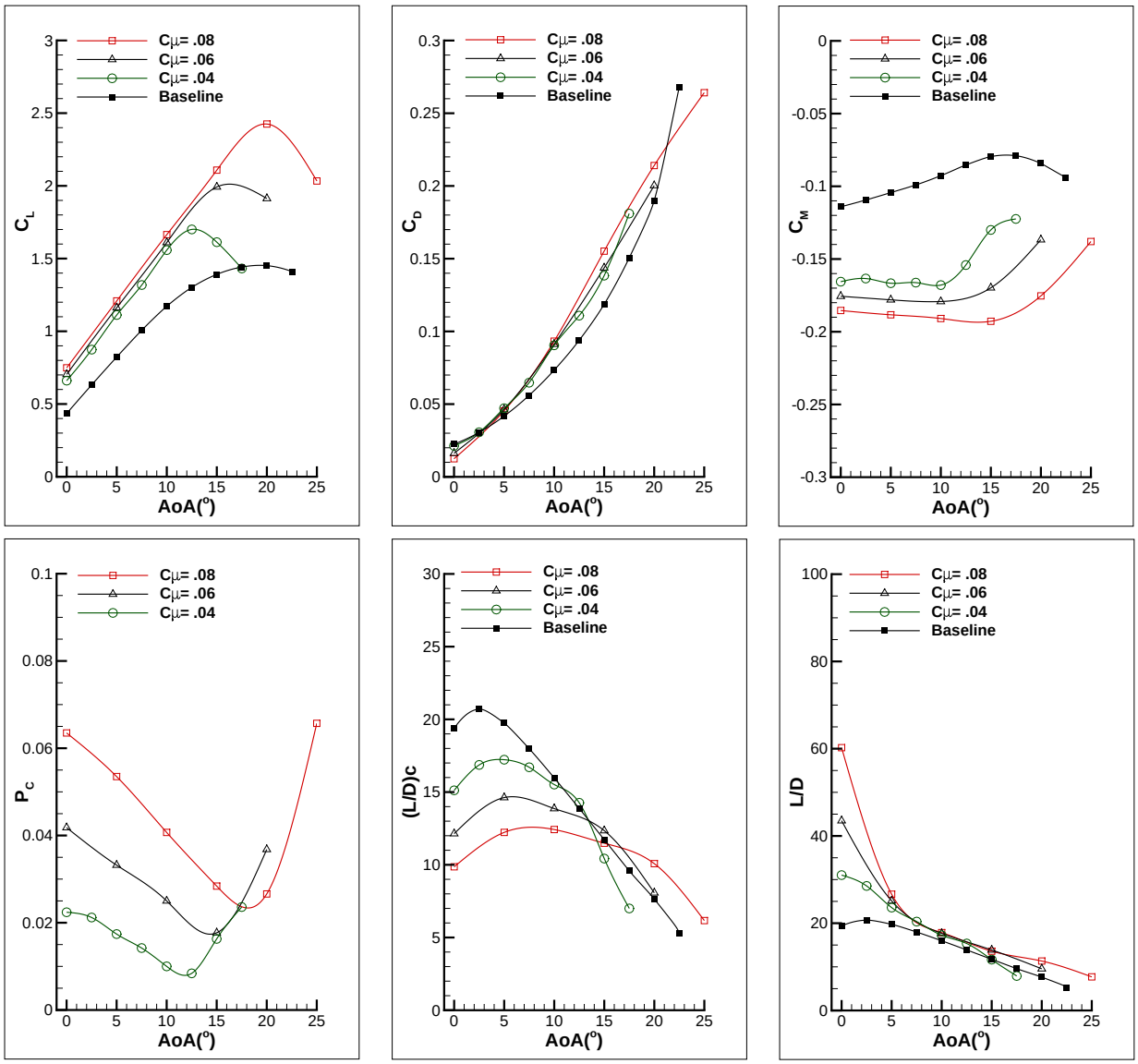

Figure 20: Forces, moment and energy expenditure versus AoA for the Design 5 CFJ wing compared with the baseline 3 airfoil. Simulations performed at M=0.15, $0.04 \leq C_\mu \leq 0.08$.

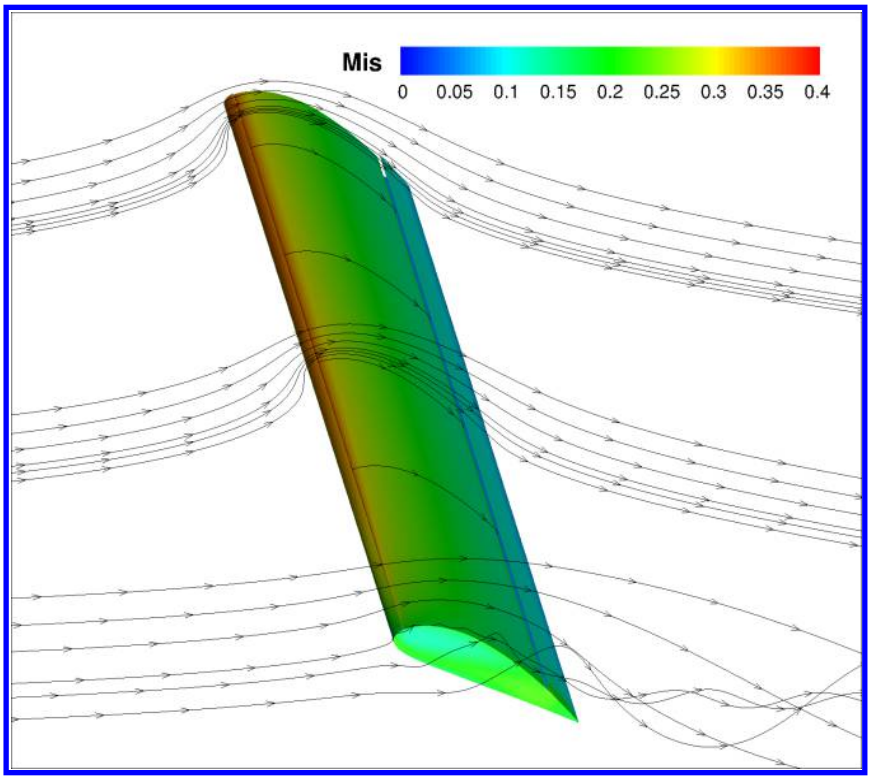

Figure 21: Surface isentropic Mach number contours with streamlines for the Design 4 CFJ wing at $AoA = 25^{\circ}$ and $C_{\mu} = 0.20$. Simulations performed at M=0.1, to simulate the takeoff and landing conditions.

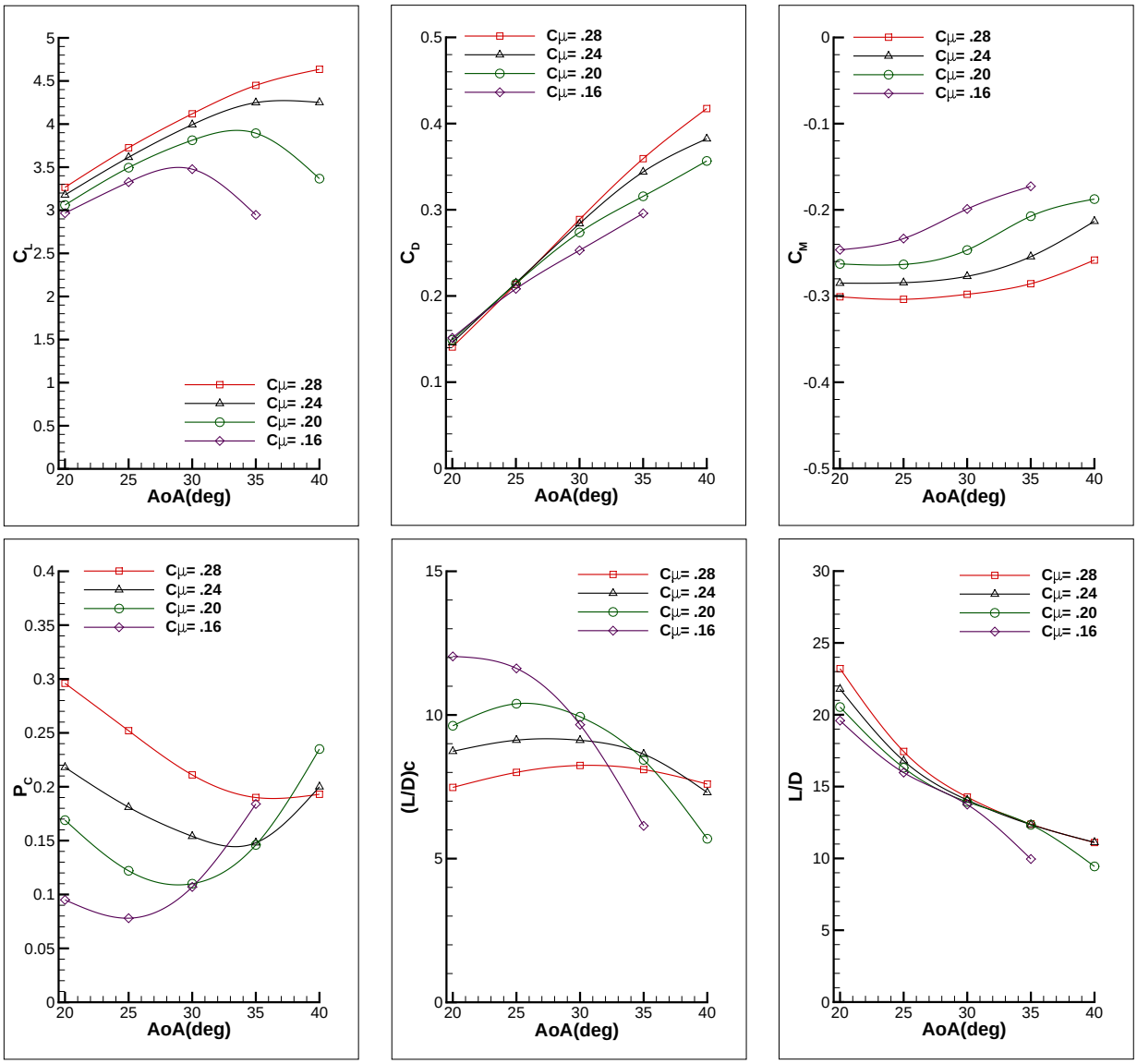

Figure 22: Forces, moment and energy expenditure versus AoA for the Design 4 CFJ wing. Simulations performed at M=0.1 and $0.16 \leq C_\mu \leq 0.28$ to simulate the takeoff and landing conditions.

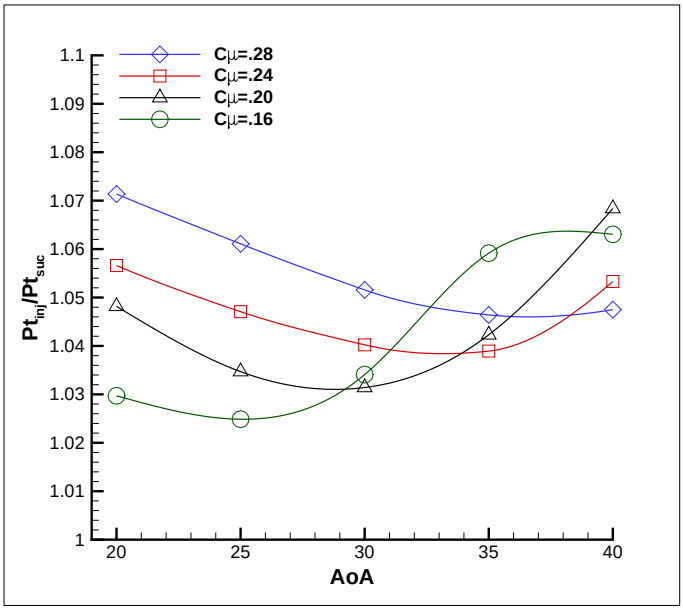

Figure 23: Mass-averaged total pressure ratio between the injection and suction cavities for the Design 4 CFJ wing for a typical takeoff or landing.

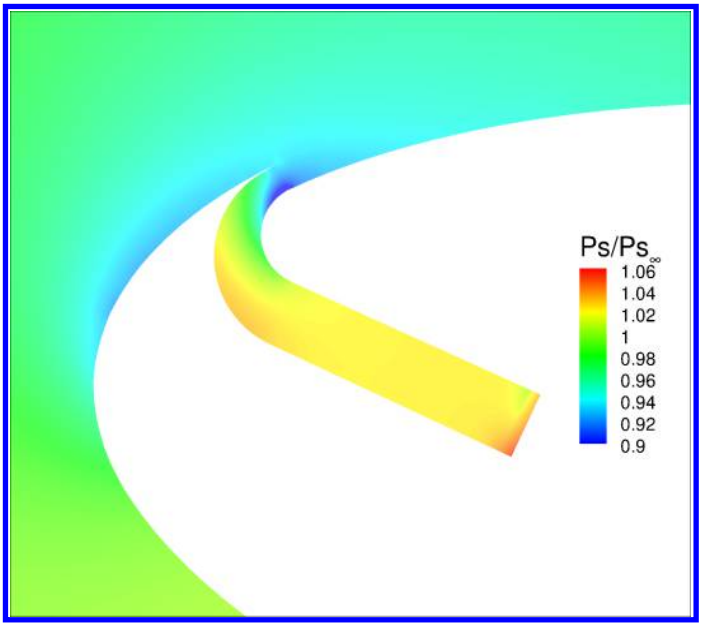

Figure 24: Static pressure contours at 50% spanwise location for the Design 4 CFJ wing. The CFJ wing is in takeoff/landing condition at $AoA = 25.0^\circ$ and $C_\mu = 0.20$. The free stream static pressure is 1.00.

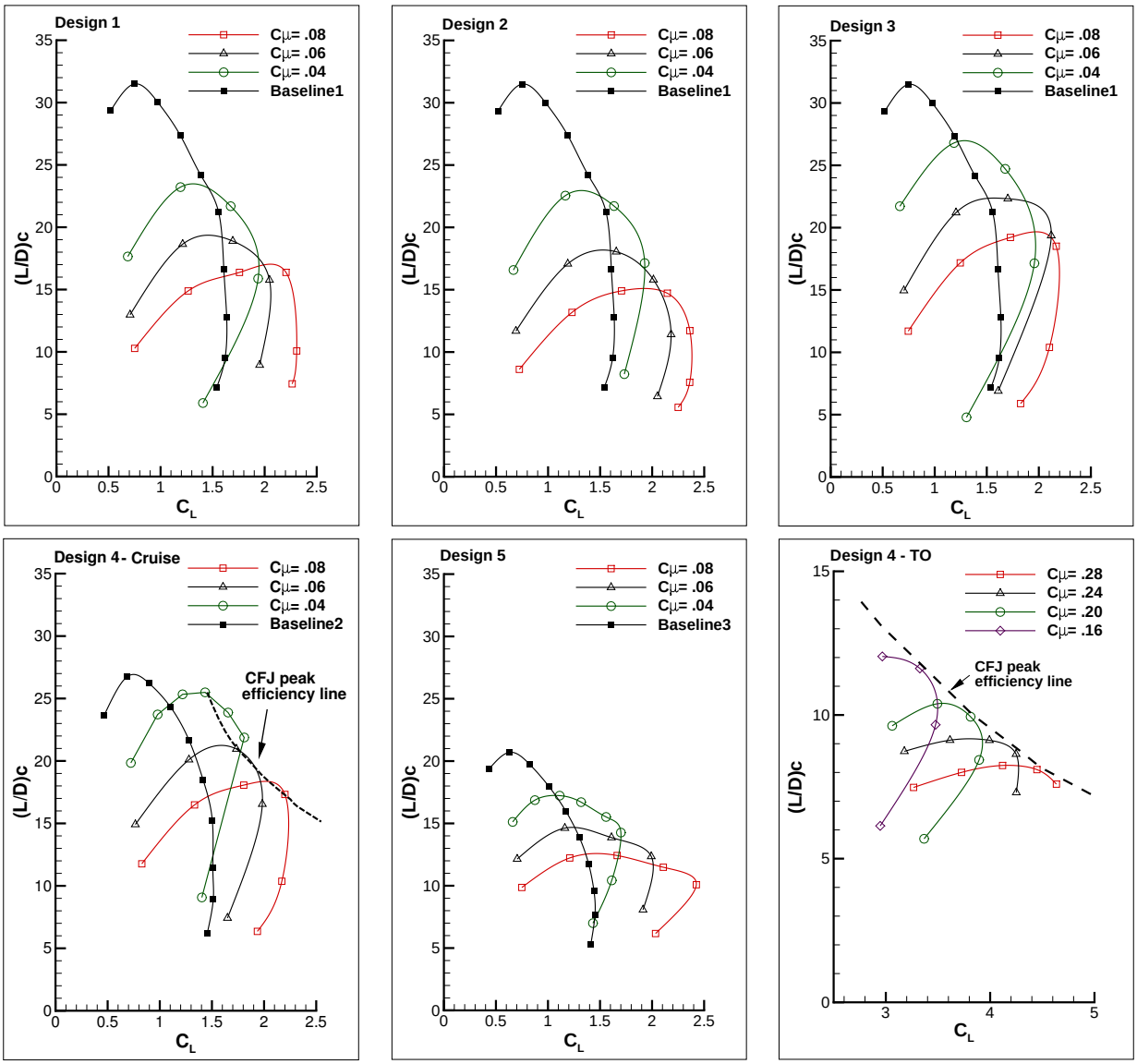

Figure 25: CFJ airfoil corrected efficiency versus C_L. Comparison between all wing studied. Simulations performed at M=0.15 with $0.04 \leq C_\mu \leq 0.08$ for the Design 1 through Design 5 plots. Simulations performed at M=0.1 and $0.16 \leq C_\mu \leq 0.28$ for the Design 4 in takeoff/landing condition.